UNIVERSITÀ DI PISA

Laurea Magistrale in Ingegneria Robotica e dell'Automazione

Tesi di Laurea

ThimbleSense: an individual-digit wearable tactile sensor for experimental grasp studies

Candidato:
Edoardo Battaglia

Relatori:
Prof. Ing. Antonio Bicchi
Prof. Marco Santello
Dott. Ing. Giorgio Grioli
Dott. Ing. Matteo Bianchi
Dott. Ing. Manuel Catalano

Anno accademico 2013/2014

Abstract

Measurement of contact forces between hand and grasped objects is a necessity for a wide array of studies on human grasping. This work presents ThimbleSense, an individual-digit wearable tactile sensor built by assembling a pair of shells around a six axis force/torque sensor. By exploiting the integration with an active marker-based motion capture system, this device also simultaneously collects information about absolute position and orientation of the fingertip, which in turn allows to obtain position of contacts and force components expressed in a global reference frame. Through use of the intrinsic tactile sensing algorithm that was first introduced in [1], it is also possible to obtain the position of contact points.

ThimbleSense can be employed to grasp a variety of objects, while still retaining the complete force/torque measurements that are generally not obtainable with other wearable approaches. This makes it a powerful and versatile measurement tool, that can be used to study various aspects of the human hand: for example investigation of force synergies, which has interesting applications in the construction of robotic hands.

Validation of the device is a mandatory step before performing novel research: in this work qualitative and quantitative validations are proposed that assess both reliability of measurements and differences with respect to bare finger grasping. It will be shown that measurements are fairly accurate, with force measurement errors of the order of 0.1 N and contact point position estimation errors of the order of the millimeter. Moreover, while the tactile feedback impairment caused by wearing rigid sheaths affects grasping, the validation experiment focusing on evaluating this effect will show significant indications that this can be overcome through training.

Acknowledgments

I would like to express sincere appreciation to my main advisor, Prof. Antonio Bicchi, who first had the idea which led to this thesis, and who offered me the opportunity to work in an excellent environment for doing research. I would also like to thank Prof. Marco Santello for accepting me as a visiting scholar at Arizona State University for six months, allowing me to experience a full immersion in an outstanding lab with a focus on neurophysiology, which immensely opened my mind.

I would also like to thank all the people working at the bioengineering and robotics research center Centro E. Piaggio, in particular Manuel G. Catalano and Giorgio Grioli, who patiently tutored me during the initial design phase, Alessandro Serio, who was an invaluable source of advice for what concerns software implementation and results presentation, and Manolo Garabini, who gave me valuable tips for what concerns the use of ANSYS. Finally, I would like to especially thank Matteo Bianchi, who, in addition to being an excellent tutor for the statistical analysis needed for an important part of the experiments, provided a final revision of all my work with endless patience.

I would also like to gratefully acknowledges Prof. Panagiotis K. Artemiadis, Bryan Whitsell, Qiushi Fu, Pranav J. Parikh, Patrick McGurrin, Keivan Mojtahedi, and Daisuke Shibata from ASU for their valuable advices and contributions to the experiments, and Andrea Di Basco from Centro Piaggio for his unique contribution in the physical realization of the device.

This work was partially supported by the European Community funded projects THE, WEARHAP and PACMAN (contracts 248587, 601165 and 600918 respectively), and by the ERC Advanced Grant no. 291166 “SoftHands”.

It pays to be obvious,
especially if you have
a reputation for
subtlety.

ISAAC ASIMOV

Contents

Chapter 1

Introduction

The human hand has a complicated structure, with a high number of degrees of freedom. Despite this underlying complexity, experimental evidence suggested through the years that, in the space of all the possible configurations, only a few basic movements (normally referred to as synergies) explain the postures assumed while grasping typical objects [2]. This concept does not apply only to postures, but also to finger contact forces [3]: the phenomenon appears to extend through the whole neuromuscular system [4]. Synergies have an immediate and practical application in the construction of robotic hands, since they can be used to simplify design and control of what would otherwise be a very complex system [5]. Measurements related to the human hand kinematics and dynamics are a fundamental prerequisite for the study of synergies. However, while several works address measurement and estimation of posture (see for example [6]-[7]), force related measurements provide a greater challenge, especially when the goal is to obtain complete information regarding both force and torque. This is often achieved by using sensorized objects [8], that can either compel grasping from predetermined locations, as in [3], or leave the possibility of a more generic grasping configuration, as in [9], even if this sometimes comes at the cost of sacrificing the number of possible contacts between the hand and the object.

An alternative approach consists in applying sensors directly on the hand, to favor versatility: this can be accomplished by using gloves (see [10] for some examples) which, however, usually use pressure sensors, and thus do not provide any information regarding shear forces. More advanced approaches exist that measure forces while leaving the fingerpad free from occlusion: in [11] the relationship between nail strain and compression forces on the fingerpad was studied, while in [12] the horizontal deformation of fingerpads was used to estimate normal forces. In [13] fingernail sensors were introduced that correlate

blood distribution under the finger nail with forces, which later publications further developed and refined (see for example [14]). This last solution is particularly interesting since it also provides measurements for shear forces; however, it requires fine calibration, and to the best of our knowledge currently provides no information regarding the position of contact points.

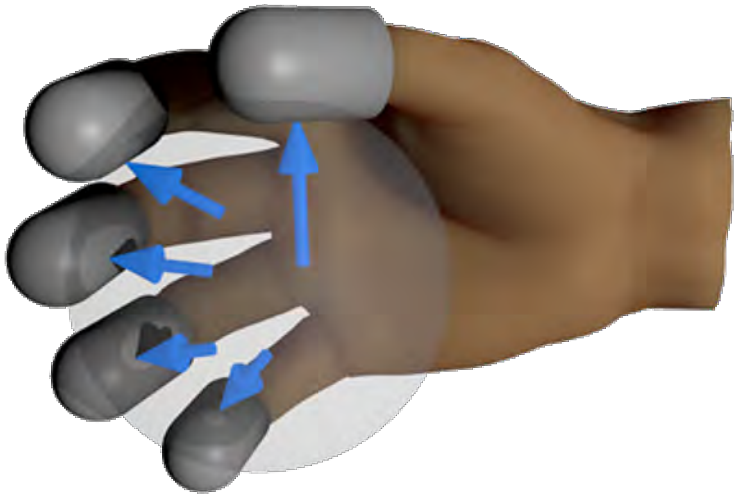

Fig. 1.1: Concept of the *ThimbleSense* digit-wearable tactile sensor.

This work presents *ThimbleSense*, a design for a sensor system which can be worn on fingertips, and gives complete measurement of all components of generalized forces applied upon grasped objects. This is achieved by combining a commercial six axis force/torque sensor with a pair of support shells, blending the two conventional approaches by building a wearable sensorized object. To obtain position and orientation of the system we integrate the sensors with a high-speed, camera-based active motion capture system, which provides a convenient and precise way to measure position. By using the algorithm proposed in [1], it is possible to determine the position on the thimble of the center of contact with the object being touched: it is worth pointing out that torque measurements are necessary to apply this algorithm. Combination of all this information provides full reconstruction of grasp forces vectors, in terms of magnitude, direction and application point.

The proposed design can also be easily applied to existing robotic hands (as shown e.g. in fig. 1.2), enabling precise online measurement of contact forces and contact position, without re-designing and replacing the usually costly hardware components of the robot.

(a) fingertip detail

(b) Whole hand

(c) Whole hand

(d) Object grasp

Fig. 1.2: Example of application on a robotic hand: the ThimbleSense wearable force/torque measuring device is placed on the distal phalanges of the DLR Hand II.

Chapter 2

Measuring the hand: state of art

The human hand is a complex system, able to perform tasks that appear simple but would be incredibly challenging for a robotic manipulator. A better understanding of how this complicated tool operates can provide invaluable knowledge to help design robotic hands, as shown in recent works (e.g. [5]). Study of human hands also have important applications in medicine, and can even provide useful insights into the inner workings of the human brain ([2],[3],[4]). It is thus no surprise that during the years measurement devices of various kind were designed to be used with human hands. In this chapter a brief survey of the state-of-art is proposed, regarding both posture estimation and force measurements.

2.1 Posture estimation

Posture estimation can be described as the problem of determining fingers orientation respect to the palm of the hand. This is generally achieved through the use of a kinematic model that allows to define a set *joint angles* for the hand: Fig. 2.1 shows two well known examples from literature. The problem of measuring posture can then be cast as an identification problem over the joint angles of the chosen model, for every position of the hand.

Many of the measuring devices are *wearable*: this means that they are systems of sensors that can be placed directly on the hand (typically gloves). Such devices can either measure the joint angles directly (Fig.2.2a-b) or measure other quantities that can then be used to derive joint angles. Wearable devices have the major advantage of being designed to adapt to a generic hand, which means that they can often be ready for use in a very short time (even if some devices, such as the CyberGlove, require a calibration for new users). However, since they usually take the form of a glove of some kind, they can

(a) 15 DoF hand model ([2]).

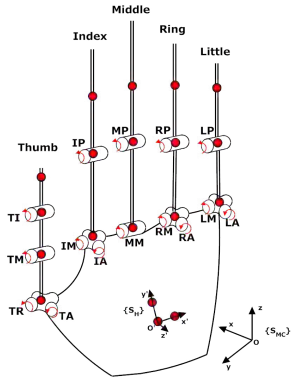

(b) 24 DoF hand model ([15]).

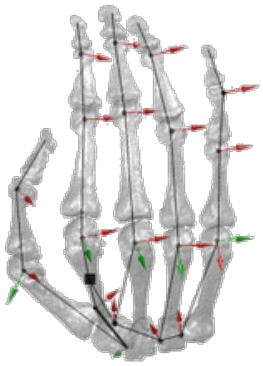

Fig. 2.1: Two relevant hand models.

(a) Cyberglove.

(b) PowerGlove.

(c) Acceleglove.

Fig. 2.2: Wearable motion tracking devices.

alter grasping respect to the bare hand condition. Also, while being able to use the same measurement device for many subjects is a positive factor, it has the drawback that precision of measurement is generally lower respect to what can be achieved with a device allowing a custom setup for each object.

(a) Example of marker-based motion capture setup ([16]).

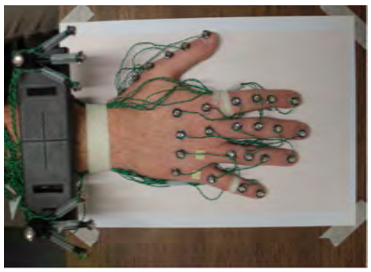

(b) Markers are tracked with a redundant number of fixed cameras.

Fig. 2.3: Marker based motion capture

A different approach to the problem of posture estimation is given by motion capture, which relies on external devices to obtain measurements from which hand posture can be estimated, and is usually vision based. Such devices may need sensors placed on the hand (commonly markers, see Fig. 2.3), or they

(a) Kinect.

(b) Hand tracking through kinect ([17]).

Fig. 2.4: Point-cloud based motion capture.

can be totally independent and acquire measurements directly (Kinect can be used for this purpose, as shown in Fig. 2.4). In the former case a custom setup is often required, which makes the acquisition process less straightforward. In the latter the procedure is simplified, but accuracy is usually lower.

Overall, human hand posture estimation is a well established topic, with several data acquisition devices that allow to obtain accurate measurements. We will see in the next section that measurement of forces is a greater challenge.

2.2 Force measurement

While posture estimation is a straightforward concept, measuring forces from hands presents different aspects. In particular, a major distinction can be made between tactile sensing and force sensing ([1]): the former focuses on measuring pressure distribution, while the latter aims to measures forces without necessarily addressing contact location and geometry.

(a) *Grip* glove from TekScan ([18]).

(b) Fingernail sensors ([13]).

Fig. 2.5: Wearable force measuring devices.

Similarly to what was observed for posture estimation, measurement devices are often wearable. Fig. 2.5a shows an example of a glove containing pressure

sensors. Measurement devices of this kind have the major advantage of providing measurements of forces of the palm, which are not easy to measure with different approaches. However, pressure sensors have their limit in the fact that they can only give normal forces.

Fig. 2.5b shows a wearable, force-based approach that uses changes in coloration of fingernails to estimate forces on fingertips. This particular device has been subject of various publications ([13],[19],[20],[21]), and has its prominent feature in the fact that it can give both shear and normal forces while leaving the fingerpad completely free from occlusion. However it gives no measurement of torques, and no way has been proposed so far to use this tool to estimate position of contacts accurately.

Force measuring devices can also be external, and they take the form of sensorized objects that can be manipulated by test subjects. This kind of approach typically uses small force/torque sensors, making it possible to obtain complete measurements. However, many of these devices have a fixed placement for the fingers, which can limit the type of grasps (Fig. 2.6a is an example). Even the devices that leave freedom of finger placement (see for example Fig. 2.6b) have a versatility limitation intrinsic in the fact that their shape is fixed. Recently more versatile objects have been introduced that allow changes to their shape (Fig. 2.6c); even in this case however it is not possible to reproduce the versatility of a wearable device that allows to grasp a generic object from everyday use.

This is the context that lead to the ThimbleSense concept: combining a six axis Force/Torque sensor with a wearable thimble, which blends the two different approaches for force sensing by creating a wearable sensorized object.

(a) Sensorized object with fixed finger placement ([4]).

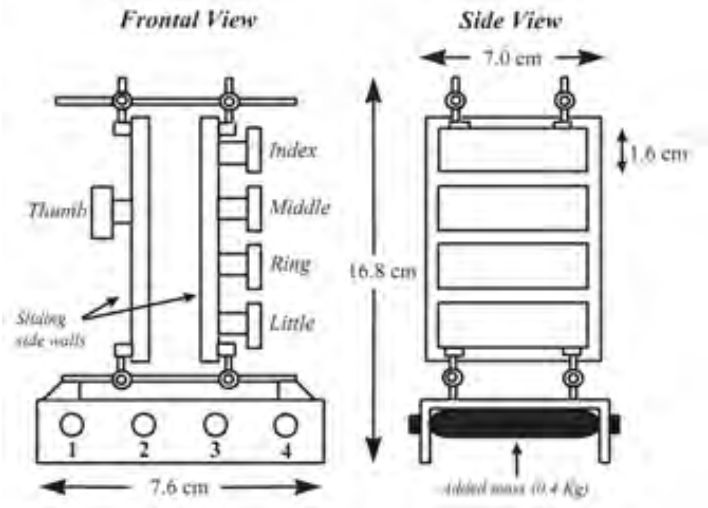

(b) Sensorized object with free fingers placement ([9]).

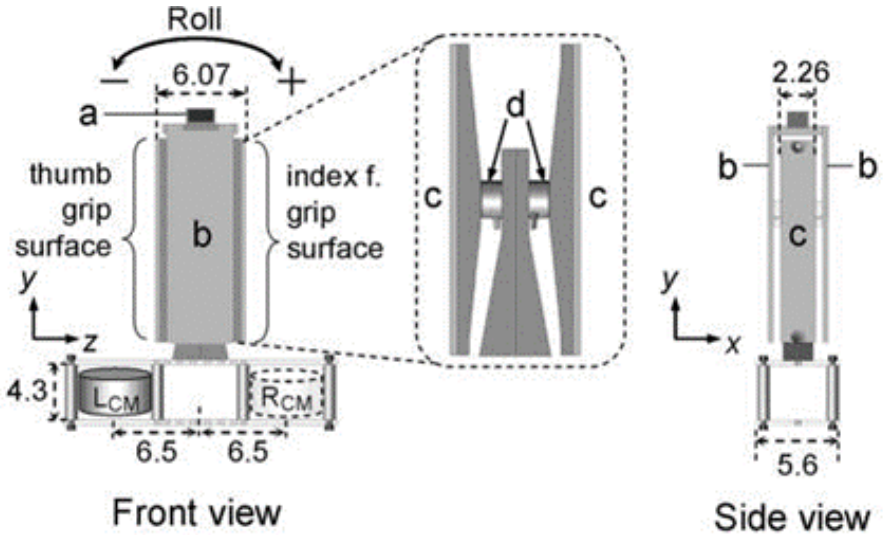

(c) Versatile tactile object.

Fig. 2.6: Force measurements through external devices.

Chapter 3

Design

In this chapter the design procedure followed is described. First the base concept that led to the creation of ThimbleSense is introduced, then the mechanical design is described in detail. Finally, integration with the motion capture system is presented.

3.1 ThimbleSense Concept

Measurement of forces and torques on a fingertip can be cast as a generic structural mechanics problem. To try and analyze the possible solutions, let us abstract from the physical problem at state, and consider the simple 2D example shown in Fig. 3.1a. A rigid body **A**, attached to a frame, withstands a force P applied on a point O at position l, perpendicularly with respect to its main axis. Let us suppose that a sensor **S** is available able to measure force F and torque M applied on its surface.

The simplest course of action to measure the applied force is interjecting the sensor between the applied force and the object **A**, as in fig. 3.1b. This solution, which is in general possible only when the position l is known *a-priori*, has the disadvantage of dislocating the point in which the force P is applied from the original O to the remote O'. This displacement could be recovered by excavating a hole inside the object **A** and using it to integrate the sensor (fig. 3.1c); or it could be removed altogether by splitting the structure in two parts, separating body **A** from the frame and interposing the sensor between them, as in fig. 3.1d. This would allow, from the measurements of force F and torque M, the straightforward reconstruction of $P = F$ and $l = \frac{M}{P}$, and thus of both the *magnitude* and *position* of the contact force. It is worth pointing out that without torque measurement it would not be possible to estimate the position of the contact.

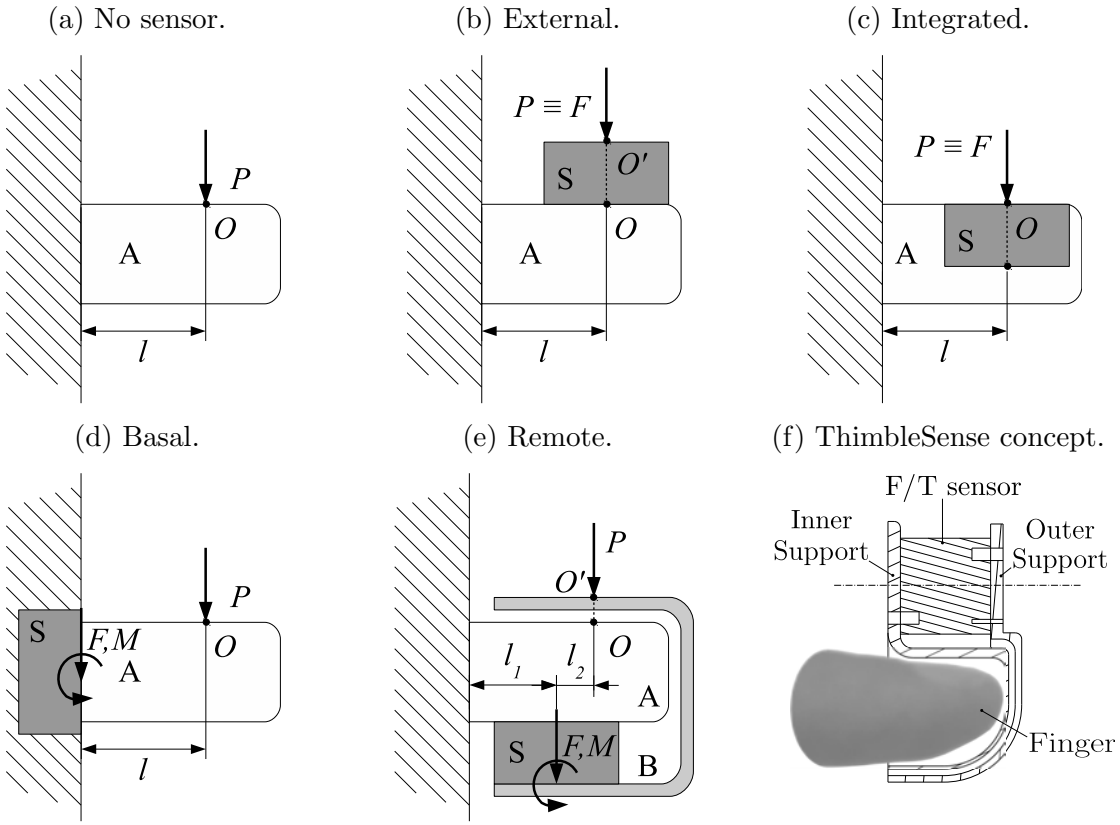

Fig. 3.1: A basic loaded structure (a), possible ways to sense the load (b-e), and the concept behind the shell-based wearable design (f).

The three approaches exposed so far lead to the design of common sensorized objects, but they can not be applied to a human finger: approaches 3.1c and 3.1d are invasive with respect to the finger, while approach 3.1b is invasive with respect to the grasp itself, owing to the typical dimensions of force/torque sensors. The problem can then be defined as designing a sensor capable of results similar to those obtainable with approach 3.1d (simultaneous reconstruction of force and contact position), which can be placed on the finger without completely altering the grasp with interposition of a cumbersome object between the finger and the contact. Fig. 3.1e shows a possible solution: by assembling the sensor **S** between the object **A** and a properly designed shell **B** we obtain a system which is completely non-invasive to the finger, while also minimizing alteration to the way the load is applied. In this regard it can be noticed that, as in solution 3.1b, the load is not directly applied on point O but on a different point O'; however, contrarily to solution 3.1b, a proper design of the shell **B** can substantially contain the distance $\overline{OO'}$. This last solution was selected for the device proposed, leading to the design of fig. 3.2.

Following this concept, a F/T sensor is assembled between an inner and an

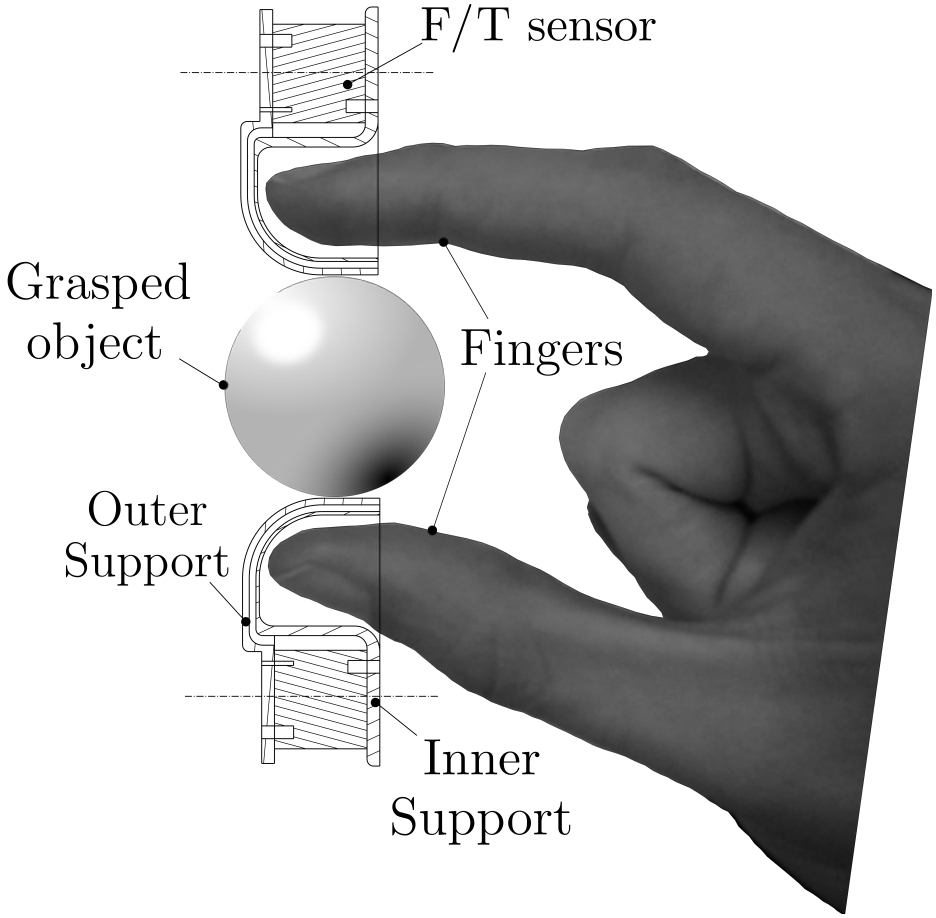

Fig. 3.2: ThimbleSense wearable device: concept

outer shell separated by a gap. The finger finds its accomodation inside the inner shell, and once the outer shell gets in contact with an object the action applied is routed though the sensor, which constitutes the only mechanical coupling element between the two shells. Owing to this a complete measurement of forces and torques can be obtained: thus, since the geometry of the external support is known, it is possible to obtain the position of the contact centroid of the loading force P, through the algorithm defined in [1] (see Chapter 4 for more details).

A number of factors must be taken into account to obtain a functional design, namely:

- *Size*: the device must be as small as possible, to minimize encumbrance. Consequently, all layers between finger and external surface of the outer shell must be as thin as possible; at the same time they need to be thick enough to keep the outer shell separated from the inner shell when a load is applied.
- *Weight*: the device needs to be light, to minimize the effort necessary to move it. For this reason a material with a high stiffness/weight ratio should be chosen.
- *Ergonomics*: the device must be shaped in such a way as to leave finger movements unhindered, as much as it is possible.

Overall, the grasping process should ideally be unaffected, and it should be possible to seamlessly place five devices, one on each finger, without them excessively interfering with hand movements and grasping capabilities. However, it is natural to expect that wearing a rigid shell over the finger will somehow alter the grasping process: this problem has been subject of study in [22], where it was shown that wearing a rigid shell on fingers significantly alters haptic recognition of common objects. A substantial part of the validation procedure presented in this paper will address this issue.

3.2 Mechanical Design

To finalize the mechanical design of the *ThimbleSense* shells, the ATI nano 17 six axis F/T sensor was selected: the sensors used in all experiments performed for this work had either SI-25-0.25 or SI-50-0.5 calibration (3.1 shows sensing ranges, the interested reader is referred to [23] for more details).

Because of its high stiffness/weight ratio, the material chosen to build the thimbles is aluminium. In order to minimize weight and encumbrance of the

Calibration	f_x, f_y	f_z	τ_x, τ_y, τ_z
SI-25-0.25	25 N	35 N	250 N mm
SI-50-0.5	50 N	70 N	250 N mm

Table 3.1: ATI nano 17 sensing ranges.

device, a Finite Element Analysis (FEA) was performed on candidate CAD models of the device, with the aim of finding the minimum thickness for the shells and the gap, still guaranteeing the shells separation when they elastically deform under load application.

To perform FEA, a load model is needed. From some basic tests performed by pressing a finger on a high precision scale, reasonable bounds of the forces applied were estimated. An average value for the force was found to be 10 N, while 35 N appeared as a superior limit. To be conservative, loads on the structure were modeled as localized forces applied on the bottom of the open ends of either the inner and the outer shell.

(a) Model of load. (b) Results.

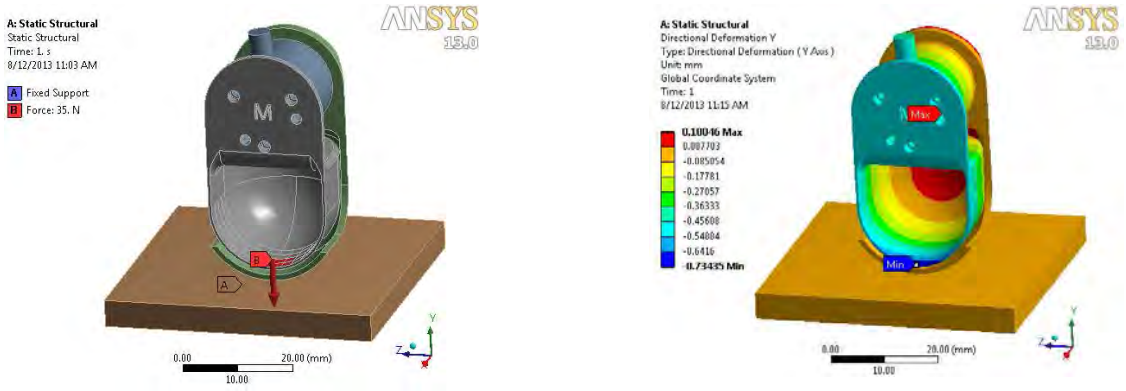

Fig. 3.3: FEM analysis: load on the inner shell.

A custom material was defined to describe the sensor mechanical properties, with elastic modulus coherent with elastic constants from the data sheet. Trials were performed for various thicknesses: we show here results for a design where thickness is 1 mm for both shells and the gap. Fig. 3.3 shows a static structural model with a localized force applied on the inner shell. It can be seen that the simulation result shows deformations smaller than 1 mm: since the load model chosen is an overestimation of the actual load, this was deemed to be adequate from a mechanical point of view. In Fig. 3.4 a load model where a force is applied on the outer shell is shown. In this case the force also presents a significant lateral component. The deformation is close to 1 mm, which is considered to be acceptable owing to the high load, and the fact that this sensor

(a) Model of load. (b) Results.

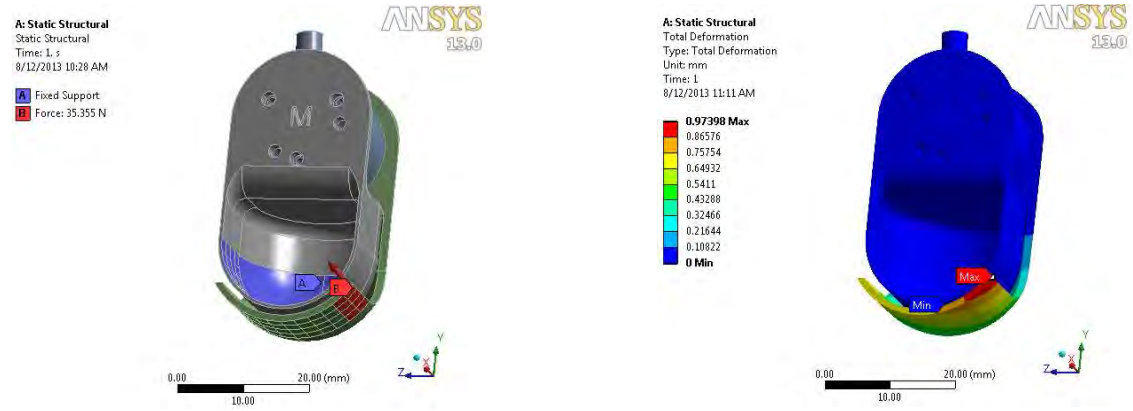

Fig. 3.4: FEM analysis: load with lateral component on the outer shell.

is designed to work with forces having a low lateral component.

(a) CAD model (exploded view).

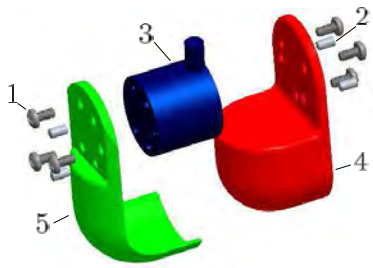

(b) Components.

Number	Name
1	6 Screws m2x4
2	6 Dowel pins 2x4
3	ATI Nano 17
4	Inner shell
5	Outer shell

Fig. 3.5: Shell based wearable device: final design.

It is worth noting that it would not be desirable to have a thicker shell, since that would cause greater weight and encumbrance. On the other hand, reducing the thickness could cause the shells to come in contact when a load is applied. The result of our design procedure can be seen in Fig. 3.5, which shows an exploded view of the final CAD model, together with the list of components of one *ThimbleSense*.

Different people have different sizes for their fingers, moreover, a significant difference in size is present also between different fingers of the same hand. The experiments in this paper are preliminary in their nature, and use a single test subject. For this reason only two thimble sizes were necessary: a larger one (25 mm diameter for the interior of the inner thimble) for the thumb, and a smaller one (21 mm diameter) for the other fingers. Designing and building additional sizes is planned as future work.

Grasping objects with a smooth, metal thimble is not an easy task due to the scarce friction. A higher friction coating is necessary to increase friction,

(a) Nitrile gloves cladding. (b) Masking paint. (c) Rubber and latex.

Fig. 3.6: Artificial fingerpad solutions.

preferably to a level comparable to human skin friction. There is more than a feasible choice for such coating: three different solutions have been tested for ThimbleSense. Fig. 3.6a shows the first, which was employed for the first prototypes: nitrile from working gloves can be used to clad the outer shell, creating an interface with increased friction and compliance. The main disadvantage of this solution is thickness, since even under load the nitrile coating is at least 1 mm thick.

In Fig. 3.6b the second solution is shown: a high friction surface can be created my mixing a masking paint with fine grain sand, and applying the mixture over some strong double sided tape. This solution allows to increase friction with a minimal thickness increase; however, the resulting coating does not offer much compliance, and it tends to lose its friction properties over time owing to smoothing from use and dust.

Amongst the three proposed solutions, the one that more closely resembles a human fingerpad is obtained with pressed rubber covered with latex (Fig. 3.6c). This solution offers compliance together with a friction that is not significantly different from the friction of a human fingerpad. However, it is less resistant to use respect to the others, and more difficult to build.

(a) First glove prototype. (b) Second glove. (c) Finger gloves.

Fig. 3.7: Interfaces used to keep the thimbles on fingertips.

The *ThimbleSense* is now designed: however, a reliable way to place it on fingertips is still needed. Ideally, we would like the inner surface of the thimble to be perfectly attached to the skin. To try and minimize the relative movement

between the device and the hand we use gloves with an interface to place the thimbles on fingertips. This interface can be as simple as glue for the ABS prototypes (Fig. 3.7a); this is not a practical solution for metal models, for which a velcro based coupling is used (Fig. 3.7b).

Fig. 3.7c shows a more advanced solution: tight finger gloves with extremities covered in female velcro work as a second skin over fingers (Fig. 3.7c), while male velcro is applied to the inside of the inner shell portion of *ThimbleSense*. The major drawback of this solution is durability, since the finger gloves tend to break when removed; however, owing to the absence of mechanical slack between finger gloves and fingers, they are the preferred solution for most experiments.

3.3 Motion Capture Integration

So far we have described a system that allows to measure generalized forces applied to a thimble, which is worn on fingertips while grasping objects. However, the measurements from the F/T sensor are expressed in a frame that is attached to the thimble itself. To locate them in a global reference frame we need a way to obtain position and orientation of the thimbles.

Position and orientation of a rigid body can be estimated from the position of a number of points attached to it [24]. Consider two sets of points $\{m_i\}$ and $\{d_i\}$, $i = 1 \dots N$, such that they are related by the equation:

$$d_i = Rm_i + t, \tag{3.1}$$

where R is a rotation matrix and t is a translation vector. Solving for the optimal transformation $(\hat{R}, \hat{t})$ which maps $\{m_i\}$ into $\{d_i\}$ requires minimizing the least squares error criterion given by

$$\Sigma^2 = \sum_{i=1}^{N} \left| d_i - \hat{R}m_i - \hat{t} \right|. \tag{3.2}$$

It is proven in [24] that a solution for (3.2) is

$$\hat{t} = \bar{d} - \hat{R}\bar{m}, \tag{3.3}$$

$$\hat{R} = VU^T, \tag{3.4}$$

where $\bar{d} = \frac{1}{N}\sum_{i=1}^{N} d_i$ and $\bar{m} = \frac{1}{N}\sum_{i=1}^{N} m_i$ are the centroids of point sets $\{d_i\}$ and $\{m_i\}$, and matrices V and U are obtained by singular value decomposition

(a) CAD model.

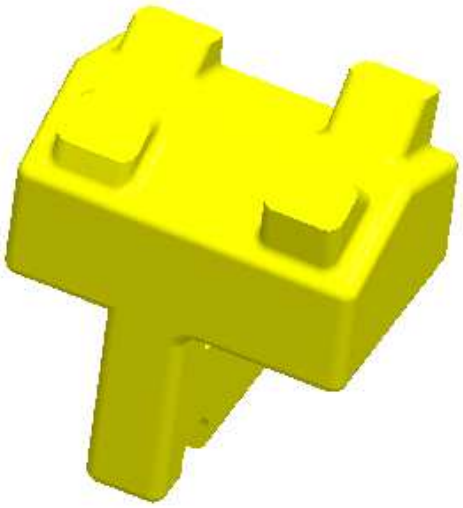

(b) Physical realization.

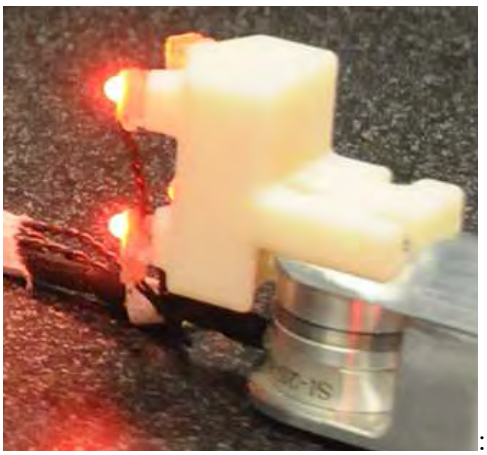

:

Fig. 3.8: ABS support for Phase Space markers.

of a correlation matrix H:

$$H := \sum_{i=1}^{N} (m_i - \bar{m})(d_i - \bar{d})^T; \tag{3.5}$$

$$H = U\Lambda V^T. \tag{3.6}$$

It is worth noting that this algorithm requires at least three non-aligned points to be effective.

Coordinates of points attached to the thimble can be obtained, for example by using a motion capture system and placing LED markers on a support attached to the thimble. The current setup uses the Phase Space motion capture system [25], with suitable ABS plastic supports to attach the led beacons to the thimbles, which are all uniquely identified by the system through an ID.

To make sure that the minimum number of three markers needed to estimate rigid body motion is always available, four marker slots were designed on the support, to be able to tolerate the occasional loss of one marker during the acquisition. Such slots are all placed at different heights over the surface of the support, to maximize visibility. The CAD model and physical realization are shown in Fig. 3.8.

Chapter 4

Contact Point Estimation

In this chapter the contact point estimation algorithm introduced in [1] is briefly discussed, and its implementation on ThimbleSense described. Not all mathematical details of the algorithm will be explored; the interested reader is referred to [1] for a more complete derivation.

4.1 The Algorithm

Object manipulation requires, for its very nature, contact between the hand and a grasped object. It is an important part of the process, and therefore cannot be overlooked by studies aiming to come to a better understanding of grasping. In [1] an algorithm was introduced that allows to estimate position of contact points from force and torque measurements, together with knowledge of geometry of the sensorized contact surface.

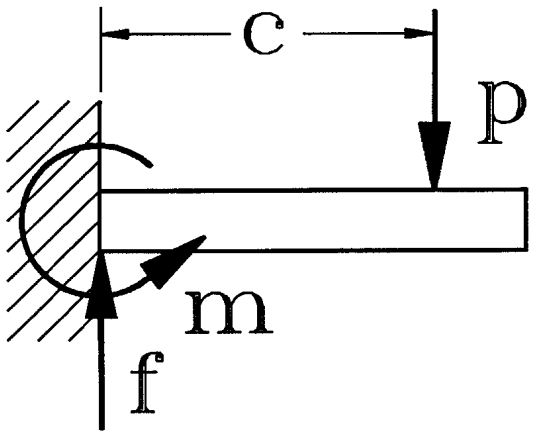

Fig. 4.1: Simple contact sensing example.

Fig. 4.1 shows a simple example that illustrates the main concept behind the algorithm. If the moment m and the force f at the fixed end of the cantilever beam are known, it is possible to find the position of contact and magnitude of the normal component of force as

$$p = f, \quad c = \frac{m}{f}. \tag{4.1}$$

Similarly, it is possible to estimate the contact location and normal force applied on a plane by measuring the force normal to it and two moments in the plane. The same concept can also be extended to non-planar bodies under certain assumptions.

This type of force-based contact sensing uses sensors that are generally placed inside the contacting surface: for this reason it is called *intrinsic tactile sensing*. Three basic contact models can be employed: the *point contact without friction*, *point contact with friction* and *soft finger contact*. The third model is the most general model to which intrinsic contact sensing can be applied, and it also the one that best models the most common case of study.

Definition of Contact Centroid
Given a surface S with an outward normal direction defined everywhere on it, and a distribution Δ of compressive tractions is applied on it, a contact centroid for S and Δ is a point on S such that a set of forces equivalent to Δ exists having characteristics:

1. It is comprised of only a force and a torque;
2. The force $\mathbf{p}$ is applied to that point, and is directed into S;
3. The moment $\mathbf{q}$ is parallel to the surface normal at that point (i.e. a pure torque about the contact normal)

The contact centroid has some useful properties. First, if contact occurs at a single point, a contact centroid coincides with that point. Moreover, even when multiple contact points and/or finite areas are in contact, the contact centroid still provides important geometric information: in particular an important property can be derived. Let us consider the plane P dividing the surface of the body in two portions and confining every contact point to one half-space, and the projection of each contact point onto P along the direction of the traction applied at the contact point itself. If all such projected points lie within the volume surrounded by the underformed surface S, then the contact centroid lies on the same side of P where Δ is applied.

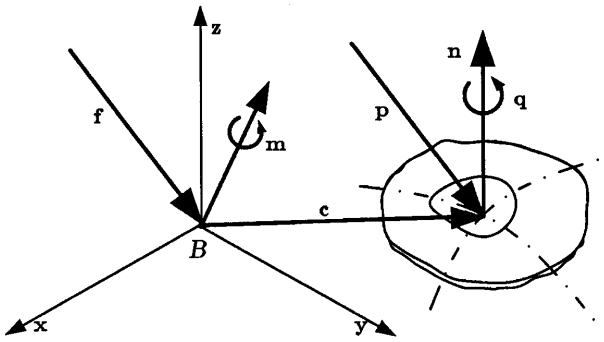

Fig. 4.2: Problem definition: vector quantities and notation.

Let us now consider the problem in a more structured way. The contact surface can be described by the implicit relation

$$S(\mathbf{r}) = 0, \tag{4.2}$$

where $\mathbf{r}$ is a point in space defined w.r.t. the frame B as defined in Fig. 4.2. If the surface S has continuous first derivatives, a normal unit vector can be defined at every point on S as

$$\mathbf{n} = \frac{\nabla S(\mathbf{r})}{\|\nabla S(\mathbf{r})\|}, \tag{4.3}$$

where ∇ indicates the gradient operator. Let $\mathbf{c}$ be the contact centroid, and $\mathbf{p}$ and $\mathbf{q}$ the force and moment applied at $\mathbf{c}$, which are equivalent to a soft finger contact. The measurable quantities $\mathbf{f}$ and $\mathbf{m}$ are related to unknowns $\mathbf{c}$, $\mathbf{p}$ and $\mathbf{q}$, by force and moment balance equations,

$$\mathbf{f} = \mathbf{p}, \tag{4.4}$$

$$\mathbf{m} = \mathbf{q} + \mathbf{c} \times \mathbf{p}. \tag{4.5}$$

For soft finger contacts the torque $\mathbf{q}$ is parallel to the unit vector $\mathbf{n}$ normal to the surface at the contact centroid $\mathbf{c}$, hence

$$\mathbf{n} \propto \mathbf{q} = \frac{K}{2} \nabla S(\mathbf{c}), \tag{4.6}$$

for some constant K.

Because of the contact centroid definition, requirements that $\mathbf{p}$ is compressive (i.e. directed into the surface) and $\mathbf{q}$ is normal to S are implicit. Expanding the equations leads to a non-linear system of ten equations in ten scalar un-

knowns, i.e. the nine components of $\mathbf{p}$, $\mathbf{q}$ and $\mathbf{c}$ and K, which can however be easily simplified into four equations in four unknowns. While it is in general not guaranteed that a solution to this system exists, it surely does if resultant $\mathbf{f}$ and moment $\mathbf{m}$ are consistent with the effects of a soft-finger type traction on S. Moreover, if a solution exists and the contact surface is convex, this solution is also unique. Unfortunately the solution to the four equations may not be trivial, but even in the most complex and general case it is possible to derive a general iterative solution.

4.2 Application on ThimbleSense

In [1] solutions are proposed for the simple point contact case, the ellipsoidal case and the general case. Moreover, solutions for some particular cases (sphere, cylinder and plane) are detailed. Here the ellipsoidal case will be briefly described, and solutions for the particular cases cited will be reported, since they were used for contact point estimation on ThimbleSense.

Let us consider a quadratic surface described by

$$S(\mathbf{r}) = \mathbf{r}^T \mathbf{A}^T \mathbf{A} \mathbf{r} - R^2 = 0, \tag{4.7}$$

where $\mathbf{A}$ is a constant coefficint matrix and R is a scaling factor used for convenience. Since reference frame B can be moved, we can assume without loss of generality that it is possible to write $\mathbf{A}$ in diagonal form

$$\mathbf{A} = \begin{pmatrix} 1/\alpha & 0 & 0 \\ 0 & 1/\beta & 0 \\ 0 & 0 & 1/\gamma \end{pmatrix}. \tag{4.8}$$

To ensure convexity (and thus uniqueness of solution) and to simplify the problem we also consider only positive definite $\mathbf{A}$ matrices, i.e. general ellipsoids. After some passages the problem can be rewritten as four equations in four unknowns in the form

$$\mathbf{\Gamma c} = \mathbf{m}, \tag{4.9}$$

$$\mathbf{c}^T \mathbf{A}^2 \mathbf{c} = R^2, \tag{4.10}$$

where $\mathbf{\Gamma} = \mathbf{\Gamma}(K) \in \mathbb{R}^{3\times 3}$ is a function of K and force components f_1, f_2 and

f_3,

$$\mathbf{\Gamma}(K) = \begin{pmatrix} K/\alpha^2 & f_3 & -f_2 \\ -f_3 & K/\beta^2 & f_1 \\ f_2 & -f_1 & K/\gamma^2, \end{pmatrix} \tag{4.11}$$

for which holds

$$\det \mathbf{\Gamma}(K) = K\left(K^2 D^2 + \|\mathbf{A}\mathbf{f}\|^2\right), \tag{4.12}$$

where $D = \det \mathbf{A}$. It can be proved that the solution to this system is

$$\mathbf{c} = \mathbf{\Gamma}^{-1}\mathbf{m} = \frac{K^2 D^2 \mathbf{A}^{-2} m + K(\mathbf{A}^2\mathbf{f}) \times \mathbf{m} + (\mathbf{f}^T\mathbf{m})\mathbf{f}}{\det \mathbf{\Gamma}}, \tag{4.13}$$

$$K = \frac{-\operatorname{sign}(\mathbf{f}^T\mathbf{m})}{\sqrt{2}RD}\sqrt{\sigma + \sqrt{\sigma^2 + 4D^2R^2(\mathbf{f}^T\mathbf{m})^2}}. \tag{4.14}$$

where

$$\sigma = D^2\|\mathbf{A}^{-1}\mathbf{m}\|^2 - R^2\|\mathbf{A}\mathbf{f}\|^2 \tag{4.15}$$

and $\mathbf{q}$ can be obtained by substitution of $\mathbf{c}$ in 4.6.

For some particular case the solution can be simplified. In particular, if we consider a spherical surface of radius R centered at the origin of the force/torque reference frame B, we have $\mathbf{A} = \mathbf{I}_3$ and $D = 1$. Hence

$$K = \frac{-\operatorname{sign}(\mathbf{f}^T\mathbf{m})}{\sqrt{2}R}\sqrt{\sigma' + \sqrt{\sigma'^2 + 4R^2(\mathbf{f}^T\mathbf{m})^2}}. \tag{4.16}$$

where $\sigma' = \|\mathbf{m}\|^2 - R^2\|\mathbf{f}\|^2$. The contact centroid for $K \neq 0$ is

$$\mathbf{c} = \frac{K^2\mathbf{m} + K\mathbf{f} \times \mathbf{m} + (\mathbf{f}^T\mathbf{m})\mathbf{f}}{K(K^2 + \|\mathbf{f}\|^2)} \tag{4.17}$$

while if $K = 0$ we can use the *wrench method* (see [1] for details) to obtain

$$\mathbf{c} = \frac{\mathbf{f} \times \mathbf{m}}{\|\mathbf{f}\|^2} + \lambda\mathbf{f}, \quad \text{with} \quad \lambda = -\frac{1}{\|\mathbf{f}\|}\sqrt{R^2 - \frac{\|\mathbf{f} \times \mathbf{m}\|^2}{\|\mathbf{f}\|^4}} \tag{4.18}$$

.

Similarly, the solution is simplified if the surface considered is a cylinder with the main axis parallel to the sensor z axis and radius R. Such surface can be described as a limit case ellipsoid for with matrix

$$\mathbf{A} = \begin{pmatrix} 1 & 0 & 0 \\ 0 & 1 & 0 \\ 0 & 0 & 1/\gamma \end{pmatrix} \tag{4.19}$$

for $\gamma \to \infty$. This leads to the following expression for K

$$K = \frac{-\mathbf{f}^T\mathbf{m}}{\sqrt{R^2\|\mathbf{f}^\perp\|^2 - \|\mathbf{m}''\|^2}}, \tag{4.20}$$

where $\mathbf{f}^\perp = (f_1, f_2, 0)^T$ is the component of $\mathbf{f}$ normal to the cylinder axis, and $\mathbf{m}'' = (0, 0, m_3)^T$ is the component of $\mathbf{m}$ parallel to the same axis. If $K = 0$ the wrench method should be applied, otherwise the contact centroid is given by

$$\mathbf{c} = \frac{K^2\mathbf{m}'' + K\mathbf{f}^\perp \times \mathbf{m} + (\mathbf{f}^T\mathbf{m})\mathbf{f}}{K\|\mathbf{f}^\perp\|^2}. \tag{4.21}$$

It is worth nothing that this solution can be generalized to a cylinder with its main axis described by a generic versor by changing $\mathbf{f}^\perp$ and $\mathbf{m}''$ opportunely.

Finally, another particular case of interest is the one given by a matrix in the form

$$\mathbf{A} = \begin{pmatrix} 1/\gamma & 0 & 0 \\ 0 & 1/\gamma & 0 \\ 0 & 0 & 1 \end{pmatrix} \tag{4.22}$$

which for $\gamma \to \infty$ degenerates into a couple of parallel planes perpendicular to the x axis of B, at a distance $\pm R$ from the origin. If we define $\mathbf{f}'' = (0, 0, f_3)^T$ as the contact force component parallel to the z axis, we can write

$$K = -\frac{\mathbf{f}^T\mathbf{m}}{R\|\mathbf{f}''\|}, \tag{4.23}$$

and

$$\mathbf{c} = \frac{\mathbf{f}'' \times \mathbf{m} + R\|\mathbf{f}''\|\mathbf{f}}{\|\mathbf{f}''\|^2}. \tag{4.24}$$

which holds also for $K = 0$. Similarly to what was observed for the cylinder case, it is possible to extend this solution to a plane with a generic normal by changing $\mathbf{f}''$ accordingly.

As can be seen in section 3.2, ThimbleSense is composed of simple geometric parts over which contact can occur: a quarter of sphere on the tip, two portions of cylinders (one at the bottom and one frontal) and, for the ABS prototype, two lateral planes. Thus, following the methodology which was proposed in [1] for compound surfaces, it is possible to find the contact point by applying solutions for the elementary geometries and checking if the resulting point actually lie on the sensor surface. Because of how the sensor is placed we also need to transform the measurements to make them suitable to apply the solutions (for example measurements need to be referred to the center of the sphere for the

spherical surface). Fortunately this can be easily done with equivalent wrench methods.

Chapter 5

Validation

This chapter presents a thorough validation of the device, for what concerns force, contact points estimation and grasping alteration.

5.1 Force Measurements Validation

The first phase of the validation procedure consisted in verifying the accuracy of force measurements provided by ThimbleSense, and it was composed in turn of two experiments. In this section we describe the first one, which used the wearable device as a scale. More in detail, two ABS supports were built. A lower support, externally covered with velcro, was placed inside the inner shell of the device, and together with a wooden platform provided an interface to place the ThimbleSense on a plane (5.1a). An upper support was fixed on the external surface of the outer shell with strong double sided tape, replacing the artificial finger pad, to provide a flat surface to put weights on (5.1b).

The experiment consisted in placing various masses on the flat surface (50, 100, 200, 400 and 600 grams), and compare for each trial force readings from the sensor with the expected nominal value of the weight force. The masses were kept on the flat surface for around 35 seconds, and average and standard deviation of measurements were computed and compared with the expected nominal values. Tab. 5.1 is a table comparing measured forces with the expected nominal values. It can be seen that measurements were virtually identical to the expected result (differences of the order of 1/100 N). With this first experiment we established that the transducers, when subject to a static load, perform correctly, and that we are processing the readings correctly.

The second experiment simulated real operating conditions by loading thimbles placed on human fingertips, validating force measurements in a dynamic test: this was accomplished by having a person lift masses with two fingers,

(a) Lower support.

(b) Setup with a mass laying on the upper support.

(c) Sample plot of measurement VS expected force, 400 g weight.

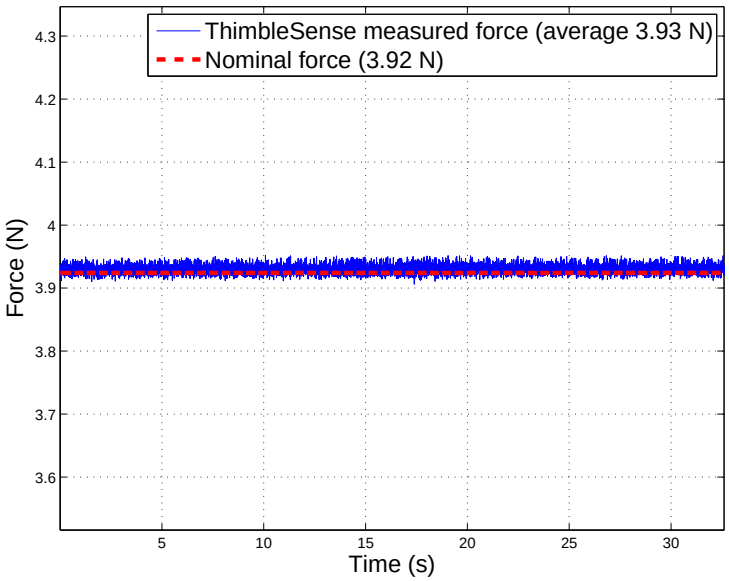

Fig. 5.1: Static weight validation.

Nominal	Measured (average)	RMSE
0.49 N	0.49 N	0.004 N
0.98 N	0.97 N	0.009 N
1.96 N	1.93 N	0.034 N
3.92 N	3.93 N	0.008 N
5.89 N	5.85 N	0.038 N

Table 5.1: Force measurement results.

while wearing the thimbles. In addition to the fact that ThimbleSense was placed on human fingertips, the main difference respect to the experiments presented in the previous sections was that the sensors were reading a force which was not static anymore, since the task involved lifting masses that moved during the experiment.

(a) Setup.

(b) Force measurement for the 400 g mass.

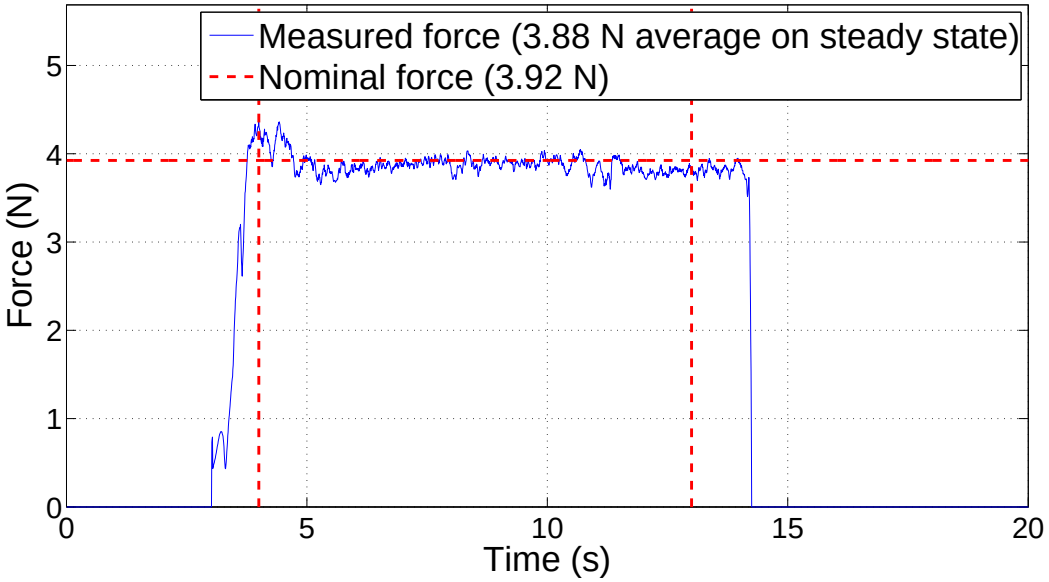

Fig. 5.2: Dynamic weight validation.

Masses lifted were 50, 100, 200 and 400 grams. Fig. 5.2 shows a picture of the setup, together with the results that are presented as a comparison between nominal expected forces and the actual measured values. The average measured force was calculated for each trial, over values recorded between 4 and 13 seconds of acquisition time, to ensure that the person lifting the masses had

Nominal	Measured (average)	RMSE (in N and % of nominal force)
0.49 N	0.48 N	0.024 N (4.9%)
0.98 N	0.95 N	0.064 N (6.5%)
1.96 N	2.02 N	0.091 N (4.6%)
3.92 N	3.88 N	0.12 N (3.1%)

Table 5.2: Force measurement results.

enough time to assume the target position. Fig. 5.2b is a plot of the complete force measurement for the 400 g mass. Tab. 5.2 shows numerical values: it can be seen that the difference between measured and expected results was at most 6.5% of the nominal value.

5.2 Contact Point Validation

Force measurements have been shown to be reliable even under dynamic conditions. In this section a third validation of the device is presented, that gives a qualitative estimation of the accuracy of force/torque measurements and of the contact point estimation algorithm. In order to do that, some medical tape was applied on the external surface of the fingertip device, with six points marked, as shown in Fig. 5.3a. The thimble was then placed on a finger, which lay on a fixed support (Fig. 5.3b)and the points were pressed with a sharp tool (a pen), in the order shown in Fig. 5.3a. Measurements were read during the task through a LabVIEW VI, with a sampling rate of 1 kHz.

Fig. 5.3 shows the results of this experiment. Fig. 5.3c shows contact points with forces applied for six samples of time, one for each target. Fig. 5.3e , 5.3f and 5.3g show components for forces and torques applied in the contact point, and contact point coordinates (for the samples where they are available), as expressed in the reference frame $\{\mathsf{F}\}$.

Intervals of time when there is a contact on the sensor surface can be clearly identified in Fig. 5.3e and 5.3g: after a short transient, contact point coordinates stabilize to a steady value. The visual feedback from reconstruction in Fig. 5.3c is realistic: to validate this numerically Tab. 5.3h shows mean values of all the components, together with variance reconstruction of initiation and termination times of the contact. It can be seen how the contact point estimate is fairly stable once the contact itself is in its steady state.

With this experiment an application of the contact point algorithm in a static case was shown. A slightly more complex validation will now be de-

(a) Sensor with marks.

(b) Setup for validation I.

(c) Reconstruction of loads.

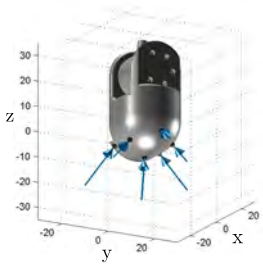

(d) Local finger coordinates {F}.

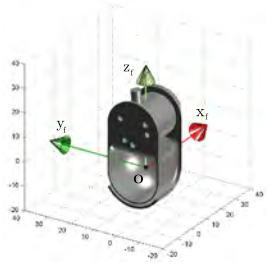

(e) Forces on contact point.

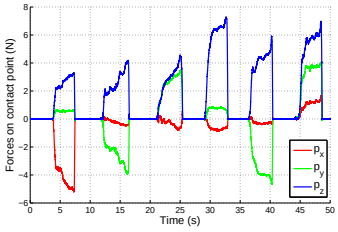

(f) Torques on contact point.

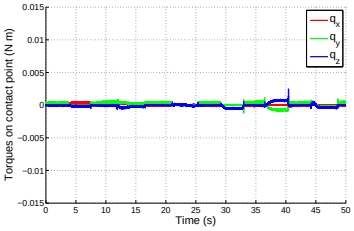

(g) Contact point coordinates in {F}.

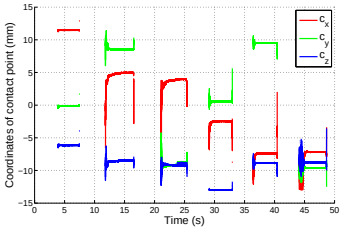

(h) Contact point statistics.

Point	Start	End	X component		Y component		Z component	
			Mean	Variance	Mean	Variance	Mean	Variance
1	4.0 s	7.4 s	11.5 mm	$1.93\ 10^{-4}$ mm^2	−0.13 mm	$5.97\ 10^{-4}$ mm^2	−6.14 mm	$6.77\ 10^{-4}$ mm^2
2	12.3 s	16.4 s	4.83 mm	$2.51\ 10^{-2}$ mm^2	8.52 mm	$1.43\ 10^{-3}$ mm^2	−8.54 mm	$7.27\ 10^{-3}$ mm^2
3	21.4 s	25.4 s	3.75 mm	$7.66\ 10^{-2}$ mm^2	−9.11 mm	$4.63\ 10^{-2}$ mm^2	−9.12 mm	$2.78\ 10^{-2}$ mm^2
4	29.5 s	32.9 s	−2.5 mm	$1.56\ 10^{-3}$ mm^2	0.56 mm	$9.56\ 10^{-4}$ mm^2	−12.98 mm	$1.68\ 10^{-6}$ mm^2
5	36.9 s	40.4 s	−7.4 mm	$8.73\ 10^{-4}$ mm^2	9.51 mm	$4.56\ 10^{-4}$ mm^2	−8.86 mm	$5.25\ 10^{-4}$ mm^2
6	45.1 s	48.1 s	−7.2 mm	$9.42\ 10^{-4}$ mm^2	−9.59 mm	$2.15\ 10^{-4}$ mm^2	−8.77 mm	$2.57\ 10^{-4}$ mm^2

Fig. 5.3: First Validation. All components are expressed in the local finger reference frame shown in Fig. 5.3d

scribed, using a KUKA robotic arm to press the thimble on a sensorized surface.

(a) Sample picture of the experimental setup.

(b) Reference frames and degrees of freedom. Subscript $_k$ is used for KUKA-attached reference frames, $_o$ for object-attached reference frames and $_w$ for the world-fixed reference frame.

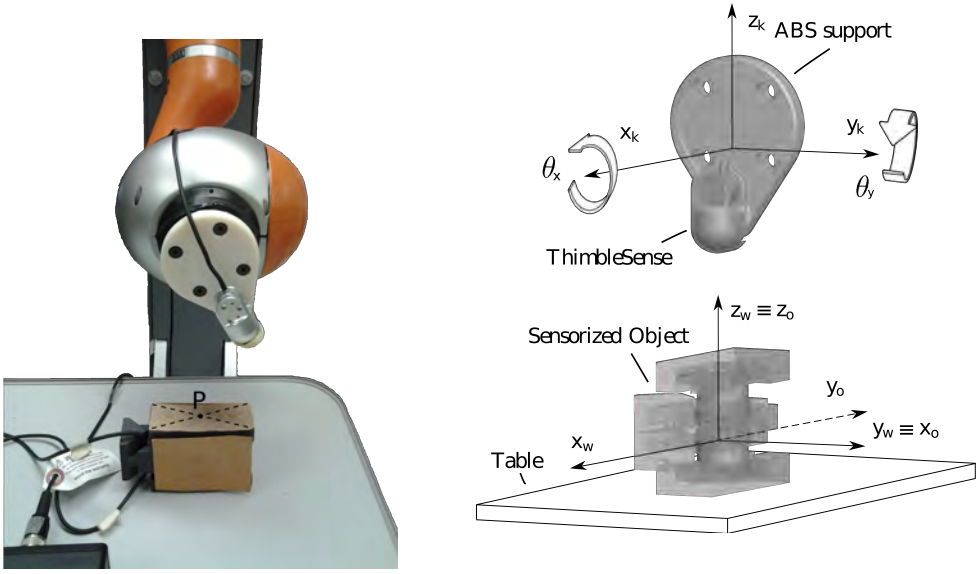

Fig. 5.4: KUKA arm validation setup.

Fig. 5.4 shows the setup: the thimble was placed on a plastic support, composed of a finger-shaped extremity covered with velcro allowing placement of ThimbleSense, and a base that could be assembled over the KUKA end-effector. A sensorized object, obtained by assembling two flat surfaces around a pair of ATI Nano 25 six axis F/T sensors, was placed on a table under the robotic arm, which allowed to obtain force and torque measurements in a local reference frame: this object is based on the same design used in [9], and is known to be reliable from previous studies (see for example [26]).

	Trial number														
	1	2	3	4	5	6	7	8	9	10	11	12	13	14	15
θ_x	-30	-25	-20	-15	-10	-5	5	10	15	20	25	30	0	0	0
θ_y	0	0	0	0	0	0	0	0	0	0	0	0	5	10	15

Table 5.3: Joint angles for each trial (degrees).

The experiment consisted in lowering the KUKA end effector gradually until ThimbleSense pressed against the sensorized surface, so that two simultaneous

readings could be compared. This was done for various values of the joint angles θ_x and θ_y, which represent rotations around x_k and y_k axes respectively: Table 5.3 shows values for every trial. The force applied was always 10 N in module. This value had been chosen from preliminary experiments that were performed during the design of ThimbleSense ([27]), which estimated the average force value on each finger in normal operating conditions.

The initial orientation had the KUKA arm keeping the z_k axis perpendicular to the plane individuated by the table surface. Trials 1 through 12 involved a rotation around the x_k axis, while trials 13 through 15 involved a rotation around the y_k axis: we will refer to these groups of trials as block 1 and 2 respectively. It is worth noting that during the first block the sensorized object was oriented as shown in Fig. 5.4a, while for the second block it was rotated 90 degrees around the z_o axis, assuming the orientation shown in Fig. 5.4b.

A major challenge for this experiment was provided by the fact that the position and orientation of the sensorized object respect to the KUKA arm were not known a priori. We were using a flat surface as support, which allowed to assume that the object was laying on a plane perpendicular to the z_w axis. Moreover, forces had a major vertical component, which reduced the impact of errors on the rotation of the object around the z_w axis. Thus, it was deemed acceptable to place the object so that it was visually oriented as in Fig. 5.4b, reducing the problem to estimating the position of the object respect to the origin of the KUKA reference frame.

The object was placed at the beginning of each block, and it stayed fixed between trials in the same block. Owing to this, it was possible to estimate the position with a preliminary calibration test. During this phase the thimble was pressed against the sensorized object while keeping both joint angles in the zero configuration: real time feedback of the contact point position on the sensorized object, as expressed in an object fixed reference frame, was available, and therefore it was possible to place the object in such a way that the contact point was superimposed to the point P marked in Fig. 5.4a.

To make the estimation more accurate, for each calibration trial we obtained, during the post-processing phase, the translation that would bring world-fixed contact point coordinates as obtained from the sensorized object onto the contact point coordinates obtained from the thimble. This translation was then combined in a homogeneous matrix with the orientation of the sensorized object, to obtain the constant rigid transformation used to identify its posture respect to the KUKA arm for the other trials.

Fig. 5.5 shows the results for this experiment. In particular, in Fig. 5.5a the

(a) Difference between estimated contact points coordinates.

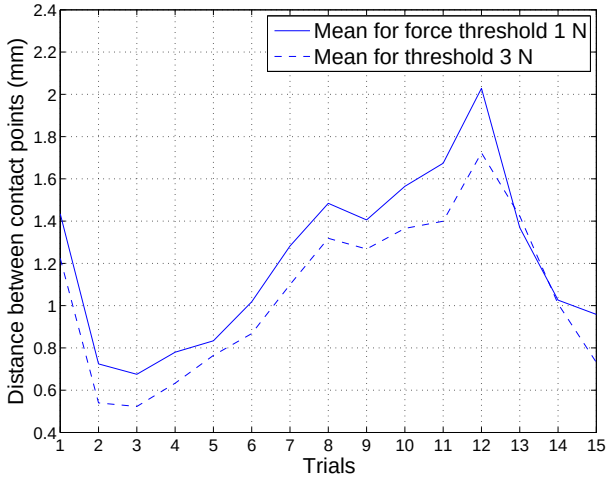

(b) Trial 12 (worst case).

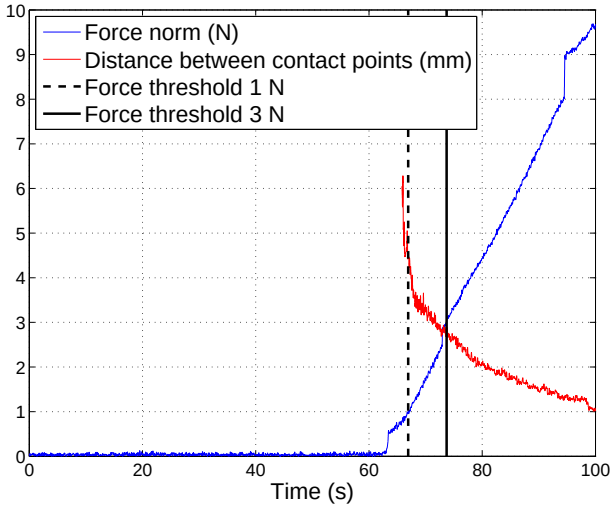

(c) Difference between force measurements.

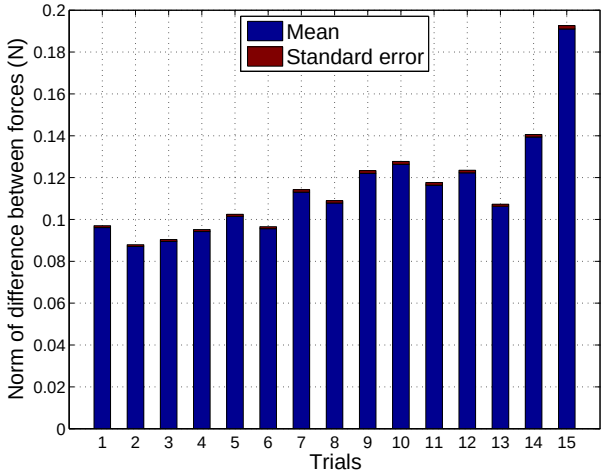

Fig. 5.5: Comparison between measurements from thimble and sensorized object.

norm of the vector difference between coordinates of the two estimates of the contact point, both expressed in the world-fixed reference frame, is plotted for each trial. The mean value has been calculated over samples for which the force norm is greater than a certain threshold: results for a threshold of 1 N and 3 N are shown. The contact point algorithm requires the contact itself to be stable to give a good estimate, which led to higher errors during the transitory phase when the thimble started touching the sensorized object: this is why higher values of the threshold tended to yield lower errors. This can be seen clearly in Fig. 5.5b, which shows data for trial number 12, for which the highest error was observed. Fig. 5.5c shows mean and standard error of the norm of difference between forces as measured from the thimble and sensorized object: it can be seen that the differences was at most of the order of 0.1 N.

(a) Flat contact interface.

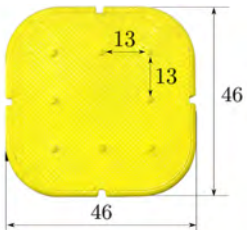

(b) Contact points reconstruction.

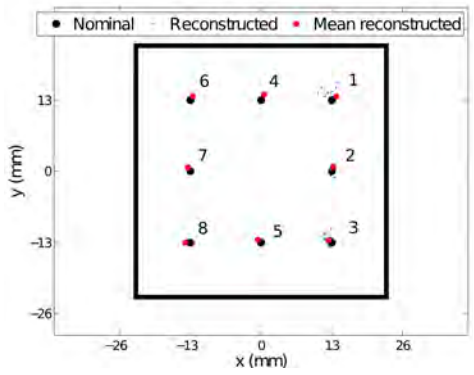

(c) Numerical data.

	Trial number							
	1	2	3	4	5	6	7	8
Mean distance (mm)	1.06	0.86	0.72	1.17	0.81	0.83	0.77	0.88
STD (mm)	0.21	0.13	0.16	0.01	0.056	0.083	0.042	0.14

Fig. 5.6: Quantitative contact points validation over a plane.

The previous experiment contained an intrinsic factor of error in the fact that the position of the sensorized object was not obtained precisely. To counter that, a third experiment quantitatively tested the performance of the intrinsic tactile sensing algorithm. A flat interface (5.6a) was constructed through rapid prototyping and assembled over an ATI 17 sensor. A number of target points were then pressed and the reconstruction obtained from the intrinsic tactile sensing algorithm was compared with the position known from CAD drawings. Results are shown in Fig.5.6b and Tab.5.6c. It can be seen that the estimation

error is of the order of the millimeter.

At the end of this section we can be confident that ThimbleSense provides reliable force measurements for static loads applied on different directions, which in turn makes it possible to estimate the contact point position accurately (the maximum average error for the worst case trial was 2 mm).

5.3 Validation with Sensorized Object

In this section another experiment is described that aimed to compare readings from the wearable device with those coming from a trusted sensorized object. Fig. 5.7a shows the setup: an inverted T sensorized object, similar to the one used in [9], was lifted while wearing the device on two fingers (for this experiment ThimbleSense was interfaced using with a fabric glove, see fig 3.7b). An unbalancing mass was placed on the left side of the object: the task required to lift it while keeping it level, meaning that a compensatory moment needed to be applied to balance the effect of the weight.

Fig. 5.7b- d show reconstruction of posture for a sample of time: in Fig. 5.7b the complete grasping setup is reconstructed, while Fig. 5.7c and Fig. 5.7d show posture and forces respectively for the wearable device and the sensorized object.

Contrarily to the work presented in [9], we are not interested in performing an analysis of learning, thus a bubble level is attached to the inverted T, in other to make the task trivial for the subject.

This task allows more detailed study and numerical comparison of forces. Quantities considered are force components tangential and normal to the object, and the compensatory moment required to contrast the action of the weight. Following the convention introduced in [9], we assume normal force to be positive when the fingers are pressing against the inverted T, tangential force to be positive when the object is lifted, and the compensatory moment to be positive when it contrasts the action of the mass. Measurements of these quantities are obtained from both devices, and compared by calculating the differences for total tangential forces (ΔF_t), compensatory moments (ΔM_c) and contact point coordinates for thumb (Δc_x^T, Δc_y^T and Δc_z^T) and index (Δc_x^I, Δc_y^I and Δc_z^I).

Fig. 5.8-5.9 show plots for these quantities. It can be seen in Fig. 5.8 a- b that, while normal forces are basically the same, there is a minor difference in values of tangential forces, which averages at around 0.5 N and decreases once a steady state is reached. This can be ascribed to the glove setup: while

(a) Grasping setup.

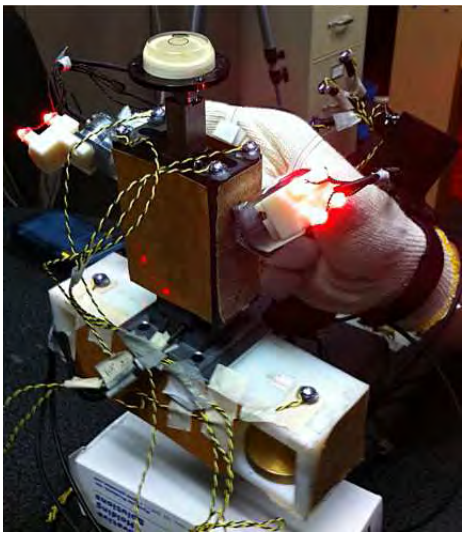

(b) Reconstruction.

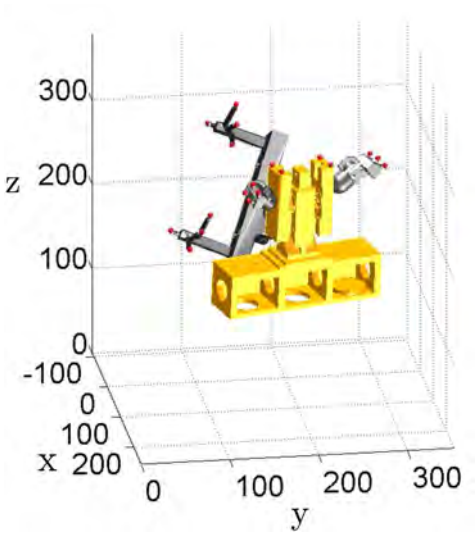

(c) Forces on fingers.

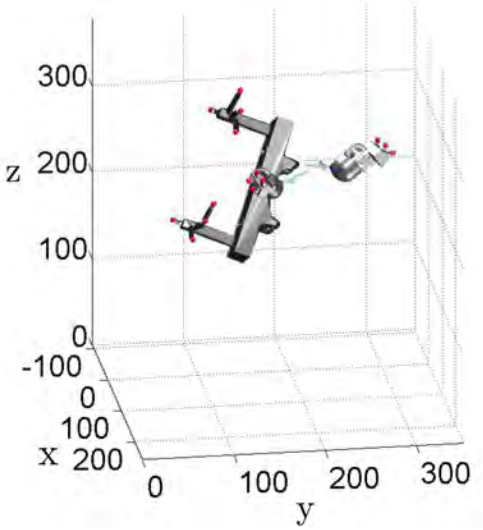

(d) Forces on object.

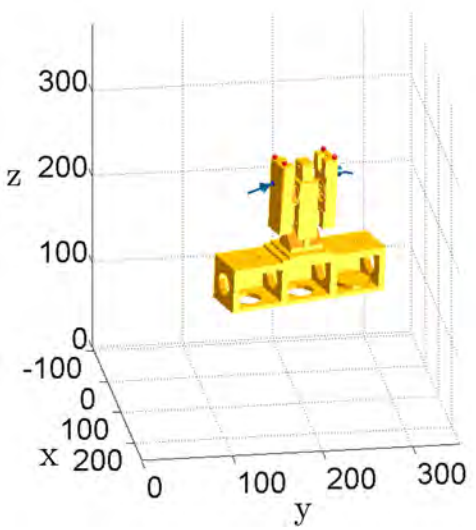

Fig. 5.7: Experimental Validation III: validation with sensorized object.

	ΔF_t	ΔM_c	Δc_x^T	Δc_y^T
Mean	0.58 N	12.67 N mm	0.28 mm	-1.50 mm
Variance	0.11 N^2	193 N^2 mm^2	0.33 mm^2	0.14 mm^2
Maximum	1.71 N	38.12 N mm	9.73 mm	3.13 mm
	Δc_z^T	Δc_x^I	Δc_y^I	Δc_z^I
Mean	1.40 mm	-3.05 mm	-4.25 mm	2.84 mm
Variance	3.52 mm^2	1.07 mm^2	0.35 mm^2	1.63 mm^2
Maximum	10.65 mm	5.18 mm	5.68 mm	6.87 mm

Table 5.4: Numerical data.

(a) Single digit tangential forces.

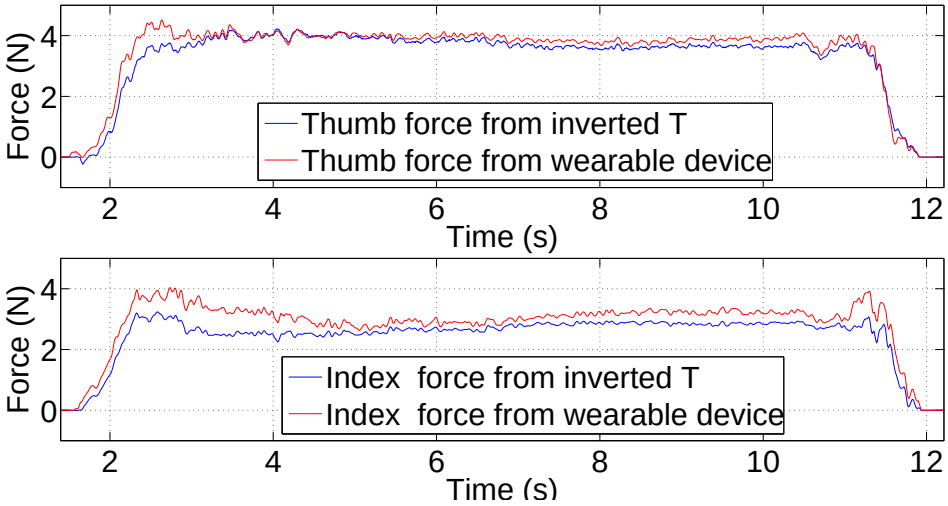

(b) Normal forces.

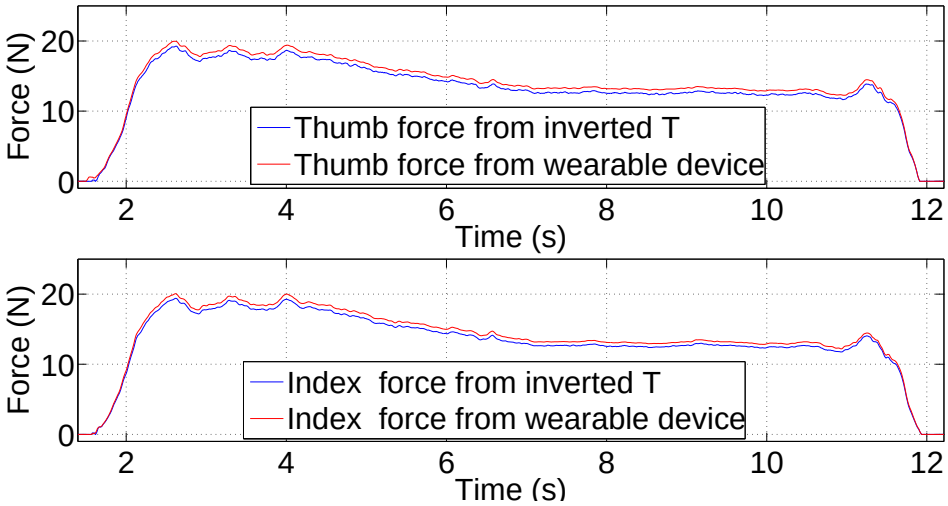

(c) Compensatory moment and lift force.

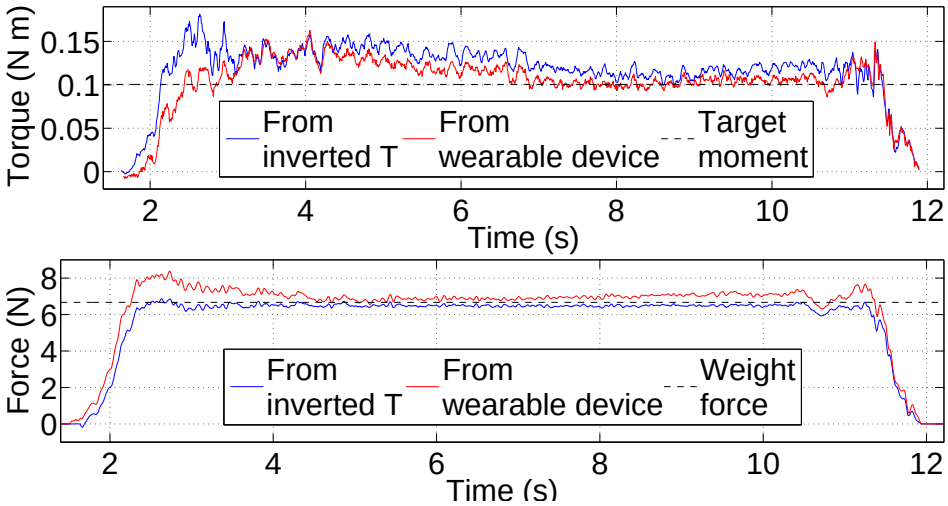

Fig. 5.8: Forces and compensatory moment.

(a) Contact point on thumb.

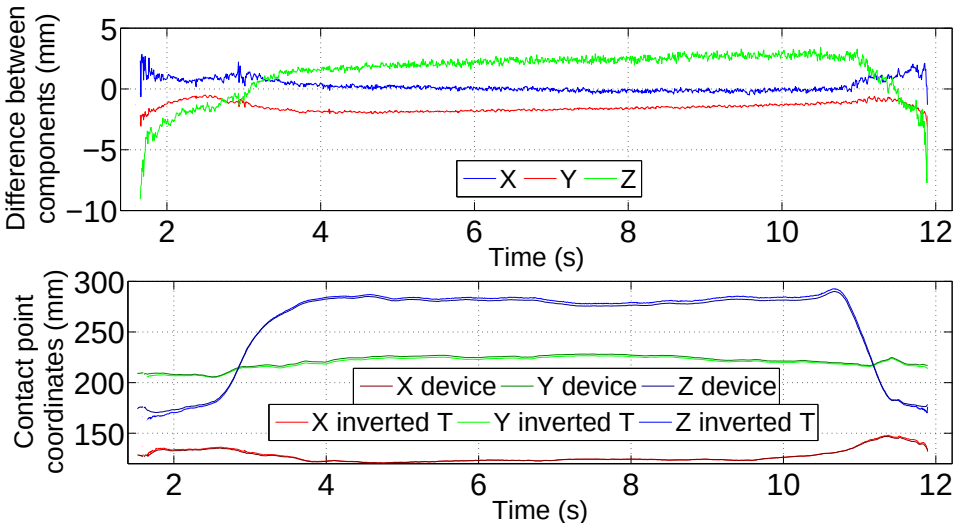

(b) Contact point on index.

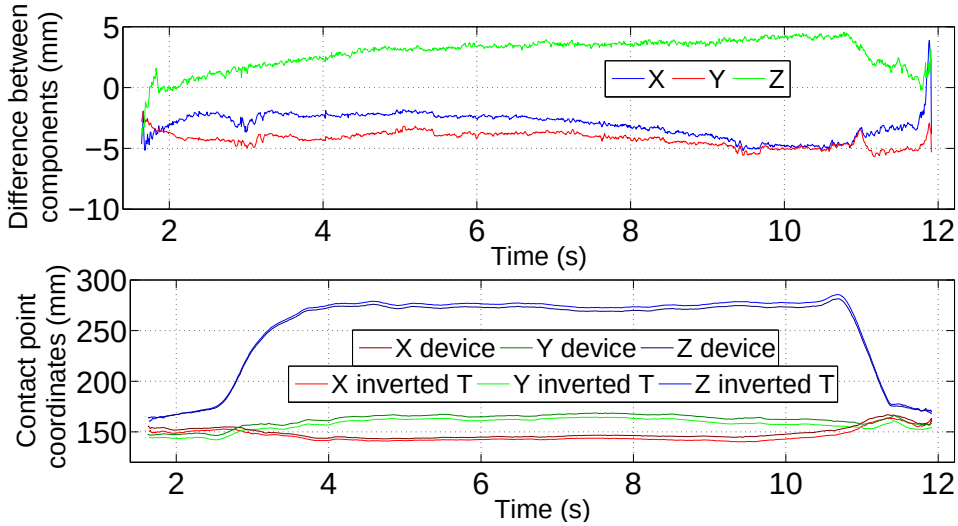

(c) Roll angle for invert T.

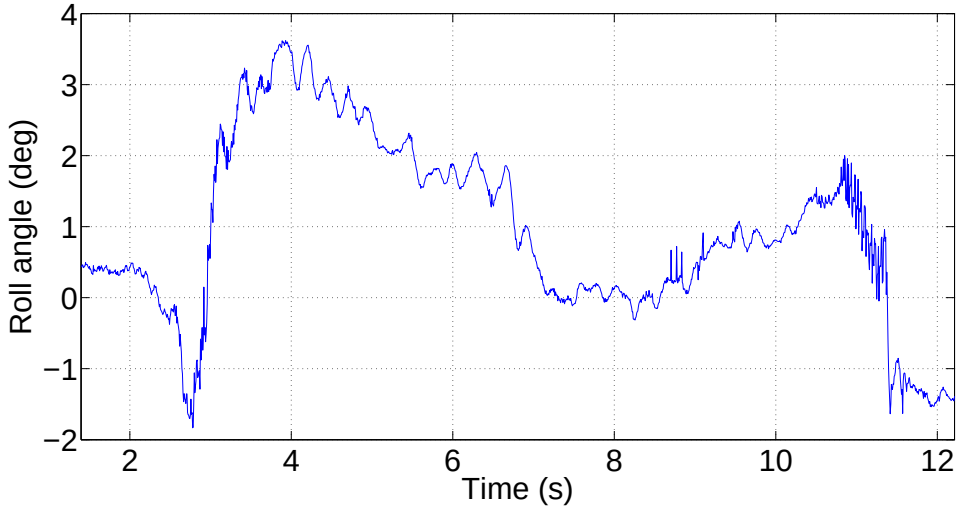

Fig. 5.9: Contact point and roll angle.

the presence of elastic bands helps keeping cables steady on the hand, it also potentially induces a distorting effect when the hand is moving and/or applying a force.

Fig. 5.9 c shows plots for compensatory moments and total tangential forces, comparing them with the moment caused by the side weight (100.5 N mm) and the force from the global weight of the object (6.67 N), respectively. The difference between values of tangential forces as measured from the thimbles and the inverted T also causes a small difference between the compensatory moments. Moreover, Fig. 5.9 a-b show that, as a consequence of differences in forces, contact point coordinates also have differences of components (a few millimeters).

To provide a better understanding of the task development Fig. 5.9 c shows the roll angle of the invert T, which is an indication of how successful the task was. In can be seen that the inclination stays fairly low: it is in fact barely distinguishable from the slight inclination of the table where the object is standing at the beginning of the task. Differences are better quantified in Fig. 5.4.

5.4 Tactile Feedback Impairment Evaluation

The experiments shown until now focused on validating the device by proving that the measurements were consistent with real data. However, there is another important aspect that needs to be analyzed: when human users wear ThimbleSense a rigid shell is placed on fingertips, thus reducing cutaneous perception and possibly altering the grasping process. In particular, since the tactile feedback from fingertips is distorted, we expect an increase of grip forces; however, as subjects use the device and get accustomed to it, we also expect them to be able to compensate - at least partially - through learning. This section describes an experiment aiming to evaluate differences in grasping when wearing ThimbleSense respect to the bare finger condition, and how learning influences the process.

The same grip device with the inverted T design described in [9] was used , with 4 LED markers added on the top to allow estimation of position and orientation of the sensorized object. The total mass of the object is 730 g, while the center of mass of the system was located in the middle. Fig. 5.10 shows the experimental apparatus: the task consisted in lifting the object using thumb and index of the right hand. In order to have an increased stability respect to the previous experiment, finger gloves were used to place the thimbles on the

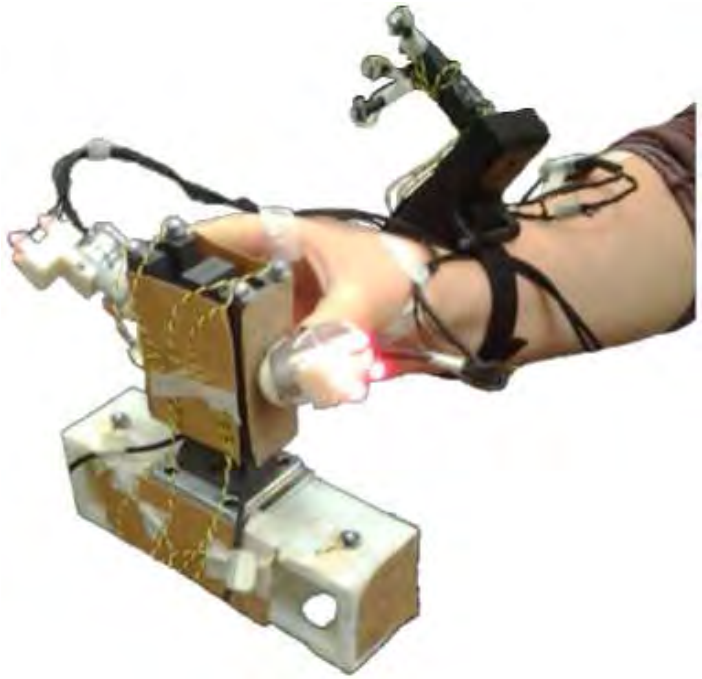

Fig. 5.10: Inverted T experiment setup

fingers.

A total of 8 subjects (7 males and 1 female, age 28.2±2.8, 5 right handed and 3 left handed) was asked to perform the experiment in two different sessions. All subjects were naive to the use of the thimbles, all had no previous history of orthopedic or neurological pathology or trauma to the upper limbs, and all gave their informed consent. The protocols were approved by the Office of Research Integrity and Assurance, Arizona State University. During the first session subjects were wearing ThimbleSense devices on their right hand, while for the second session they had to perform the same task with bare fingers. Both sessions had a total of 30 trials, and at least two days were interposed between them. Breaks were allowed at will, and a one minute break was imposed after the 15th trial, to avoid fatigue. The fact that all subjects kept using the right hand in both conditions is why we accepted left handed subjects for the experiment.

Data analysis focused on evaluating the effect of cutaneous information loss, by comparing steady-state grip forces in the two different conditions. However, large differences between the two static friction coefficients (respectively of bare fingers and latex artificial finger pad against the sandpaper covering the inverted T object), may also concur in determining different normal forces. We asked a male right-handed subject (27 year old), who had no neurological or physical impairment that would have affected the experimental outcomes,

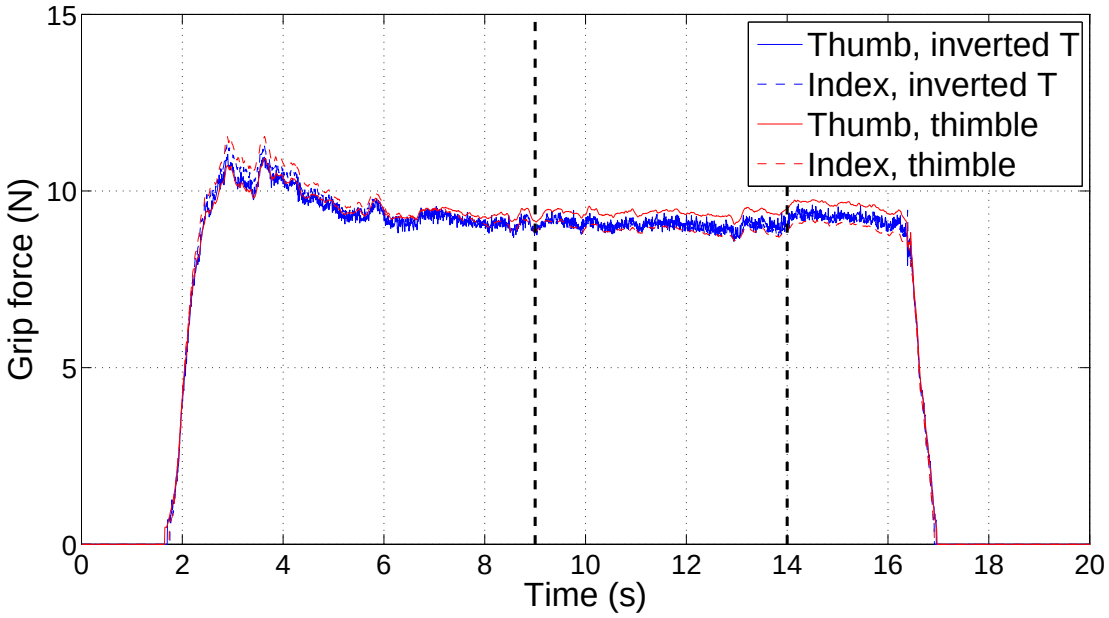

Fig. 5.11: Grip force data for a representative trial.

and who did not participate to the main experiment, to perform 5 trials of a standard slip test in order to get a ball-park estimation, following a procedure similar to the one described in [28]. The average value obtained for the bare finger condition (1.20) is analogous to the one reported in [28], while the average value obtained with the ThimbleSense devices was 1.17. This result led us to neglect the difference in the friction coefficient between the two experimental conditions in the successive force analysis.

Fig. 5.11 shows the grip force plot for a representative trial. Since we were interested in steady-state values of the force, we considered a time window of 5 seconds for each trial, under which the contact between fingers and the object appeared to be stable, and calculated the mean grip value for that trial as the average of measurements in this range. This was done for every trial and subject, for both conditions. The result is a range of plots similar to those shown in Fig. 5.12- 5.15: as we expected, the average grip force starts higher when wearing the thimbles compared to the bare fingers condition. However, it can be observed that mean grip forces when wearing ThimbleSense also tend to decrease over the trials, which for some subjects yields a final value that is comparable to the one obtained with bare fingers (Fig. 5.12 and Fig. 5.15), while for other subjects the value stays higher (Fig. 5.13 and Fig. 5.14).

We attempted to quantify the learning rate in two different ways. One is by interpolating linearly the mean grip across trials, which provides the slope of the linear model for forces F as function of number of trials n_t, $F = \alpha\ n_t + \beta$,

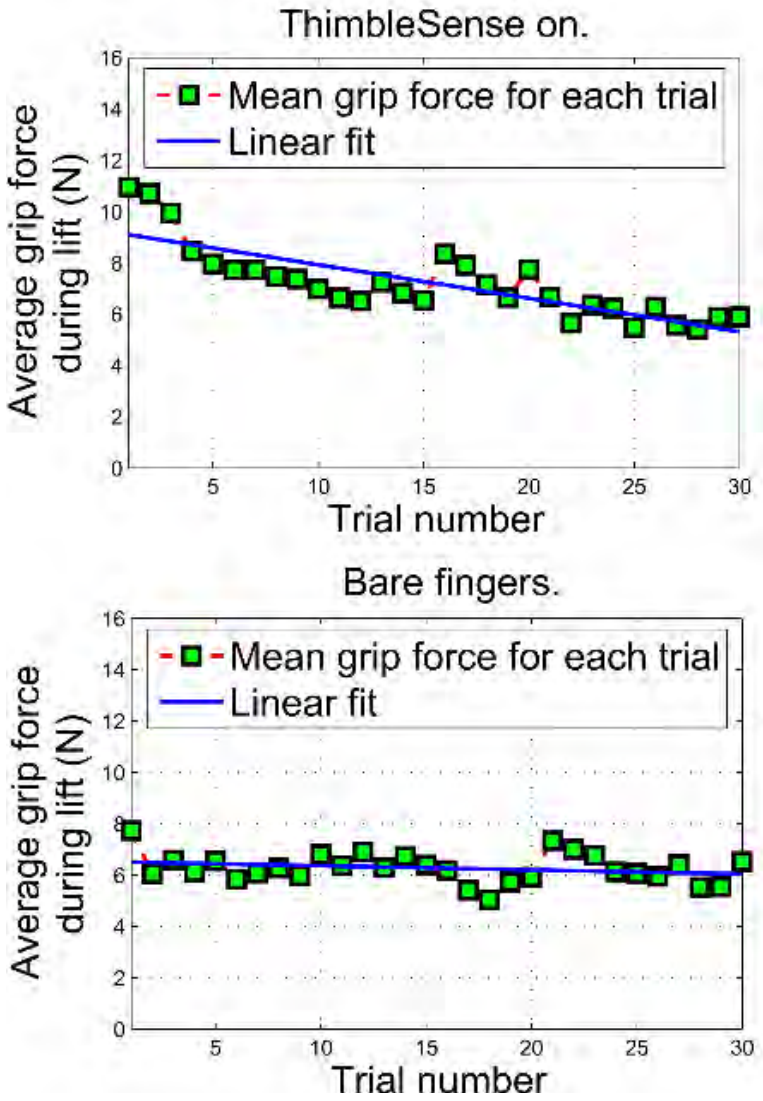

Fig. 5.12: Subject 3 (right-handed).

as a numerical indication of learning. Tab. 5.5 shows numerical results of this operation for all subjects under the two different conditions. It can be seen that the slope α is always higher when wearing ThimbleSense, and p-values show that the value of this slope is always statistically significant, except for three subjects under the bare fingers condition (which is caused by the fact that for these subjects forces immediately go to steady state values when lifting the object with bare fingers).

The second way of quantifying learning is evaluating grip forces during the last trials. Fig. 5.16 shows a bar plot comparing the average of the mean grip over the last ten trials under the two different conditions, for every subject (subjects 1 to 5 are right handed, while subjects 6 to 8 are left handed). As was already observed when comparing the sample plots of mean grip over number

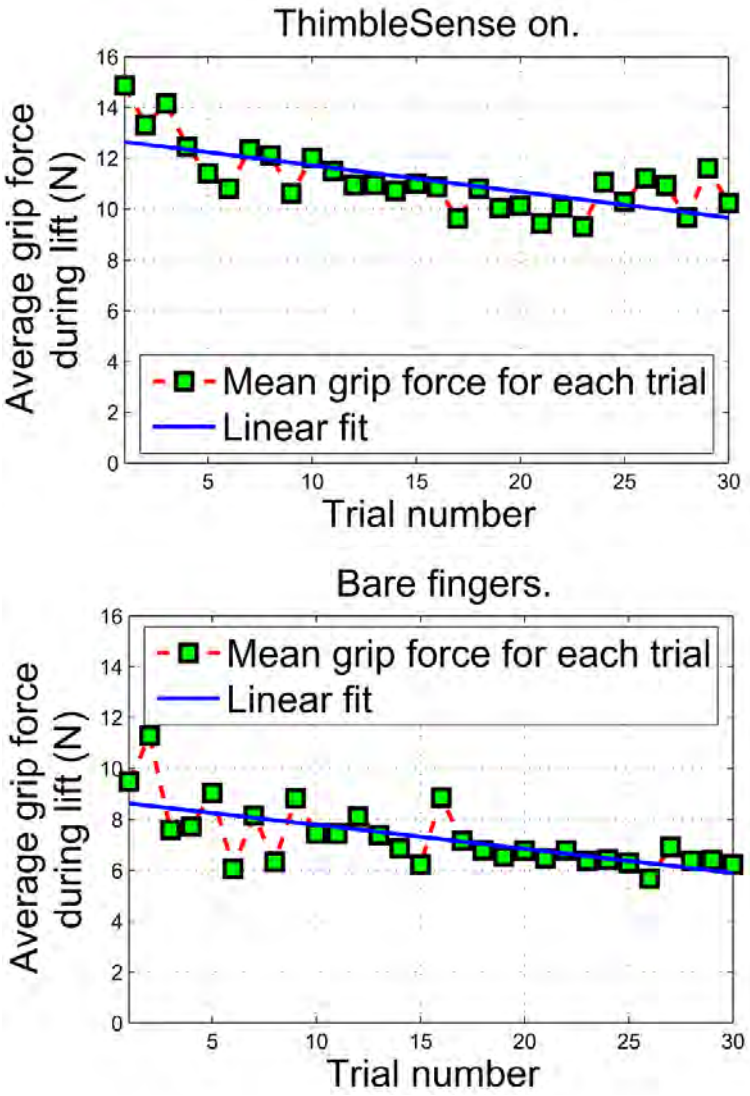

Fig. 5.13: Subject 5 (right-handed).

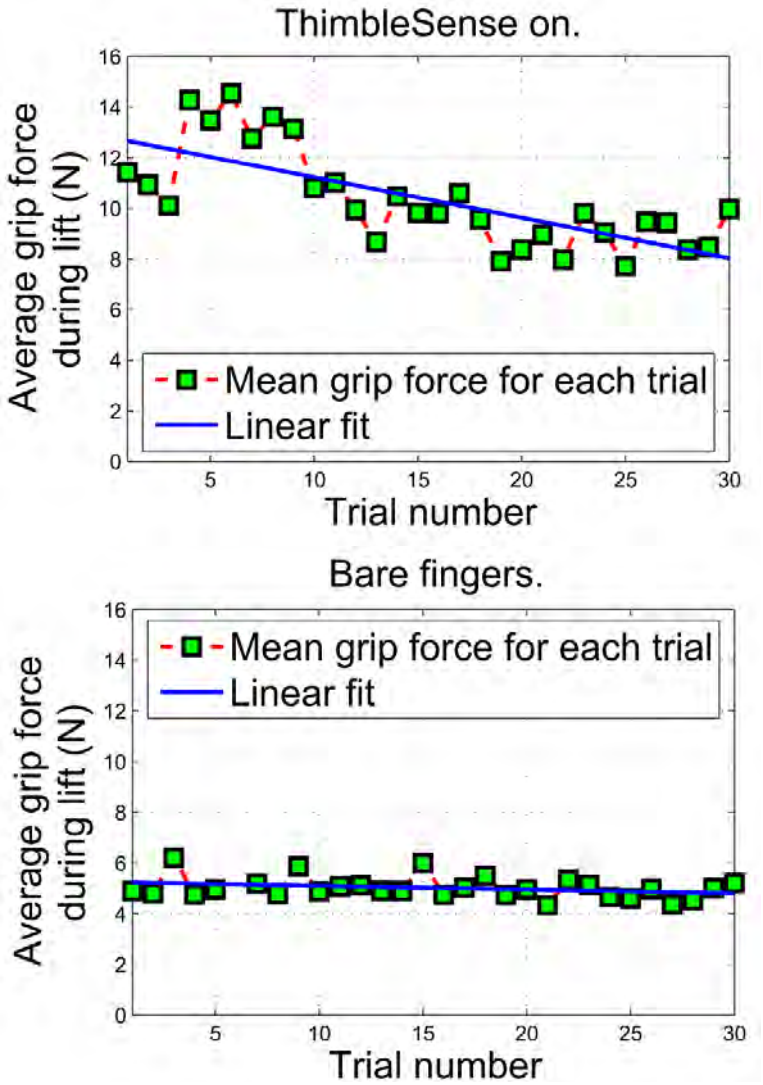

Fig. 5.14: Subject 6 (left-handed).

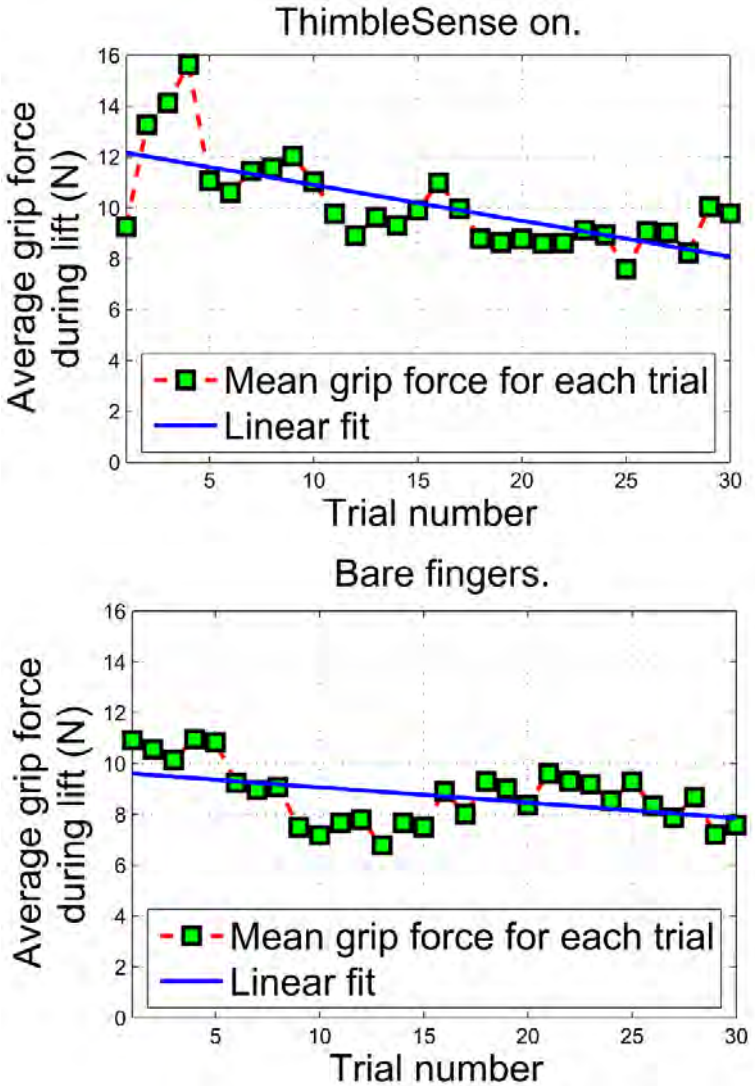

Fig. 5.15: Subject 7 (left-handed).

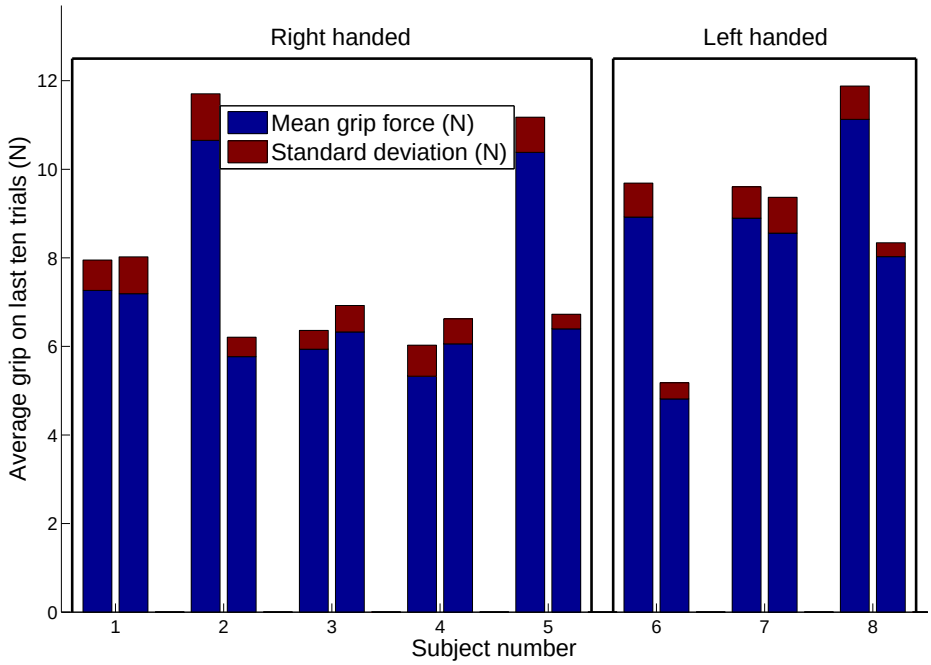

Fig. 5.16: Average of the mean grip on the last ten trials for each subject. There are two bars for each subject: the first bar represents values while wearing ThimbleSense, while the second bar is for bare fingers.

of trials, the result was not the same for every subject: the first, third, fourth and seventh subject had comparable values for the mean grip over the last ten trials in the two conditions, while the other half retained a significantly higher grip force. Moreover, for the subjects that concluded the block with similar grip force values, further analysis showed that they were also not statistically different (5.6).

This result gives indication of the fact that at least half of the test subjects were able to adapt to the distortion of tactile sensation for what concerns grip force control. For the other half, two possibilities were open: they could have been unable to adapt the force control to the distorted tactile sensation, or they may have been in need of more practice with ThimbleSense to be able to control grip forces properly.

In order to further investigate this aspect, a third block of trials was proposed to subject number 2, for whom the gap between the final values of grip force in the two conditions was the highest. During this third block the subject was asked to repeat the task while wearing the thimbles, but the number of trials was increased to 60 instead of 30, to provide to the subject more time to adapt. To reduce the effect of task-related learning from the previous experiments, this third block was recorded after some time: the number of days that passed between the execution of the second block and the third was 11, while

(a) Thimbles on, first block (30 trials).

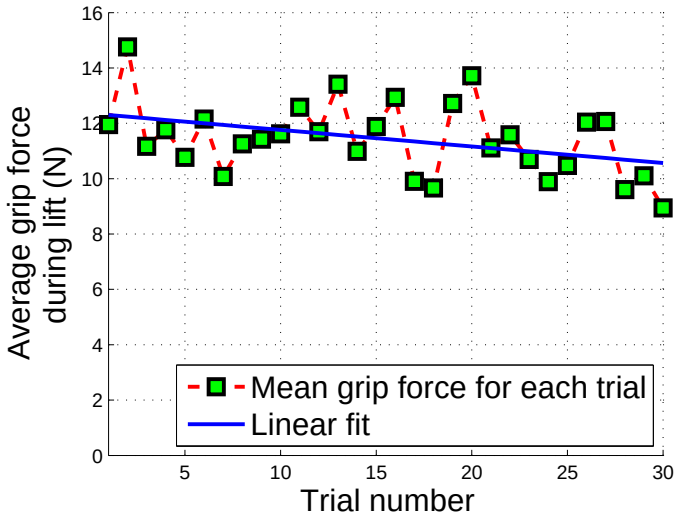

(b) Bare fingers, second block.

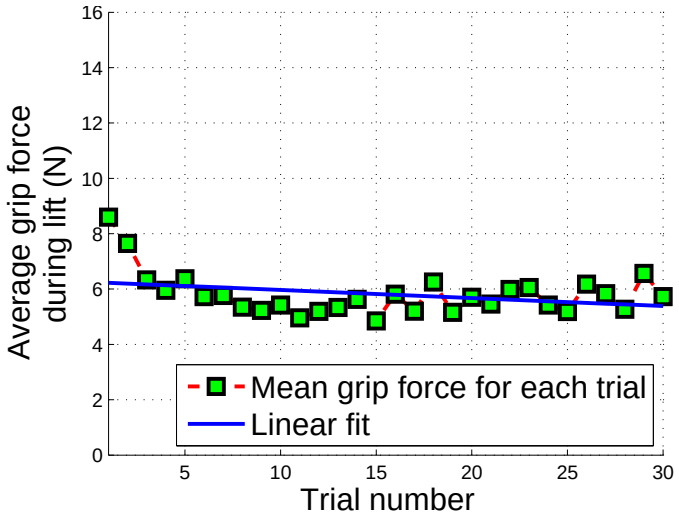

(c) Thimbles on, third block (60 trials).

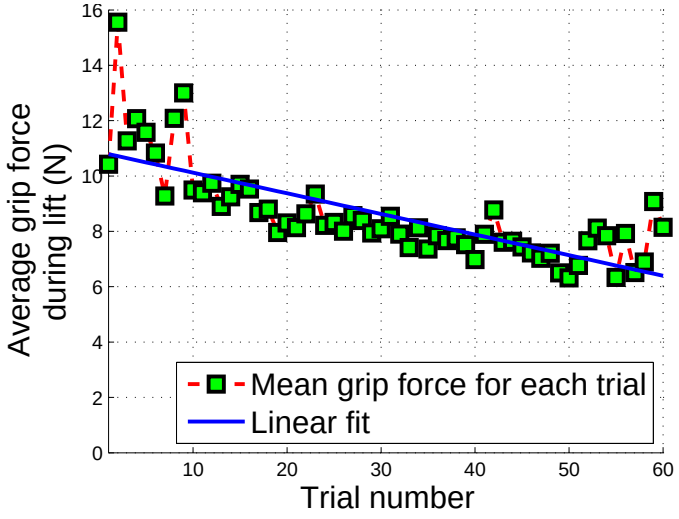

Fig. 5.17: Comparison between the three blocks of trials performed on subject 2.

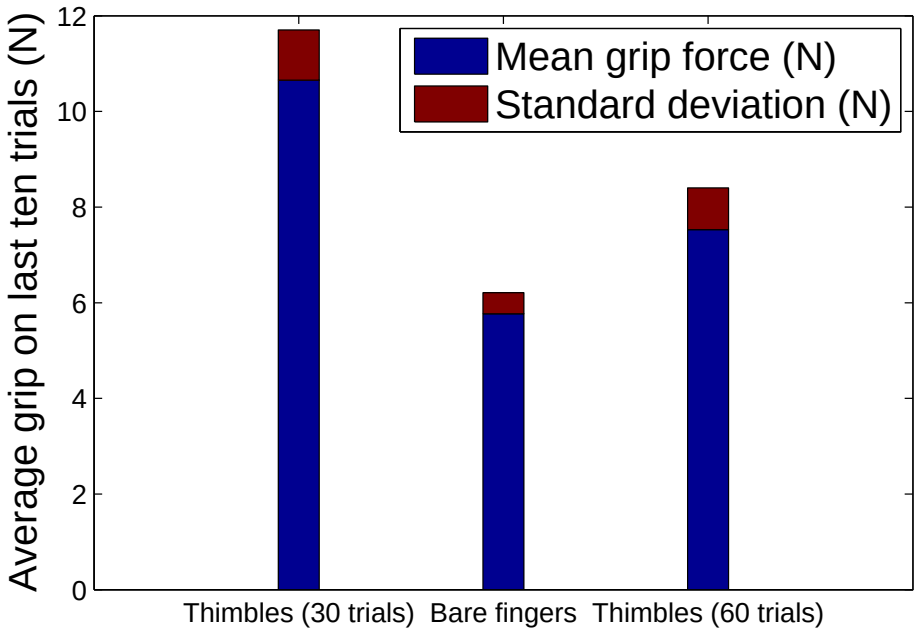

Fig. 5.18: Comparison of the average of the mean grip on the last ten trials for subject 2 for the three different blocks.

20 days passed between the execution of the first and third block.

Fig. 5.17 shows plots of the mean grip over trials for subject 2, for all three blocks of trials, while Fig. 5.18 is a bar plot representing the average of mean grip on the last ten trials for each block. What is noticeable is that the final average value of force, while still higher than the final value of grip force in the bare fingers condition, was considerably smaller than the value that was obtained in the first block. Most importantly, comparing plots for the first (Fig. 5.17a) and third (Fig. 5.17c) blocks of trials it can be seen that the grip force decreased more rapidly for this last block (which can be quantified numerically by comparing values of α in Tab. 5.5 and 5.7). The initial force β was also smaller. Therefore, there is evidence that the subject was able to learn not only from repetition of trials (α coefficient significantly lesser than zero), but also from the previous practice with ThimbleSense (smaller initial force respect to the first block, which was carried in the same condition as the third).

5.5 Sample Experiment

This second experiment shows a qualitative reconstruction of postures of the thimbles and of applied forces. For this purpose, a subject wears the *ThimbleSense* while executing five tasks that involve objects of different shapes. The

five tasks are designed to carry different degrees of challenge for the device. Fig. 5.20 shows the objects used for the five tasks with main dimensions (in mm), as well as the task execution and the reconstruction of the contact forces and positions. Please refer to that figure for the following discussion.

(a) Ball. (b) Cup. (c) Bottle.

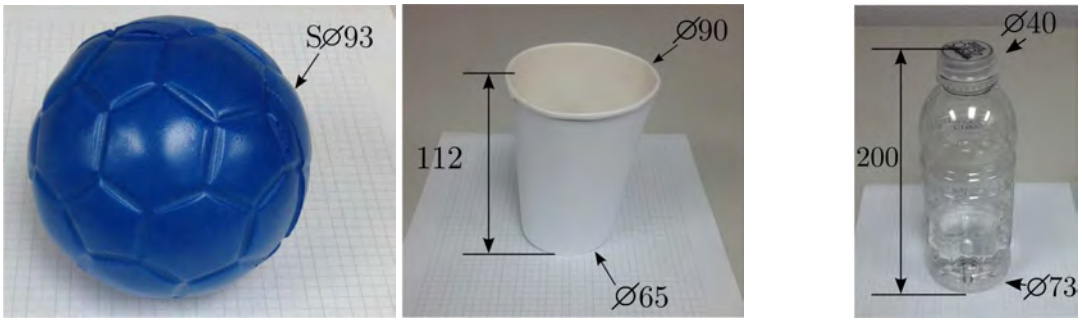

(d) Coin. (e) Egg.

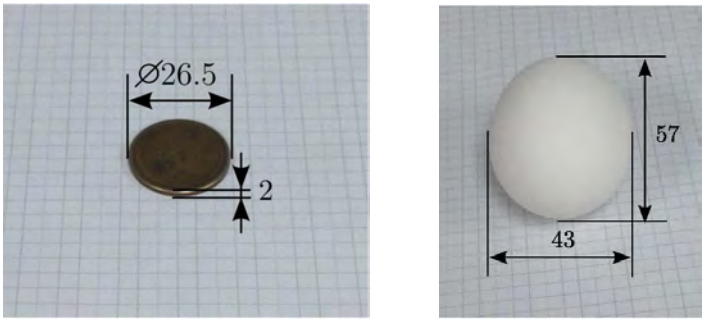

Fig. 5.19: Experimental Validation II: objects.

The first task is a basic one: the subject is simply required to lift a light (46.7 grams) ball. While this task does not present a particular degree of challenge for the device, it can be interesting to see in Fig. 5.20f the opposition between the force applied by the thumb and forces applied by other fingers.

The second task has the subject lift a soft paper cup partially filled with water (mass 168.8 grams). The challenge is slightly higher for this task, since more careful control of forces is required to avoid excessive deformation. As in the previous task, the reconstruction seems plausible and opposition can again be noticed between the force exerted by the thumb and those by the other fingers.

In the third task a partially filled bottle with a screw cap needs to be opened (mass 251.3 grams). The degree of challenge here is substantially higher compared to the first two tasks, since a nimbler movement needs to be performed to open the bottle. Fig. 5.20h shows reconstruction of postures and forces: view from the bottom allow to notice how the three forces act in order to exert a

(a) Ball grasp.

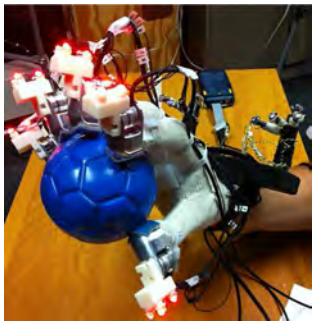

(b) Cup grasp.

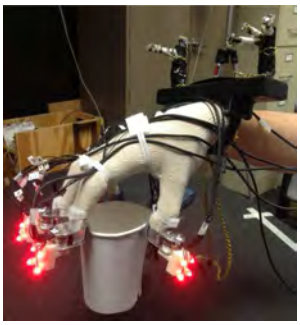

(c) Bottle grasp.

(d) Coin grasp.

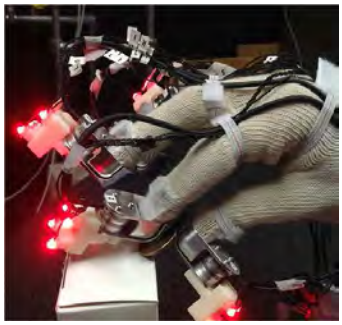

(e) Egg grasp.

(f) Ball reconstruction.

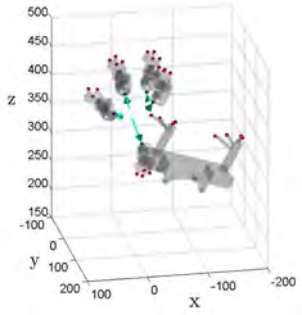

(g) Cup reconstruction.

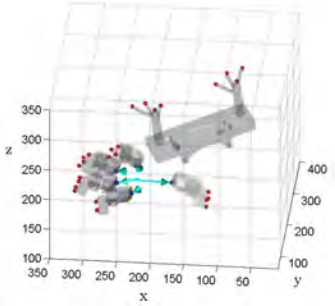

(h) Bottle reconstruction.

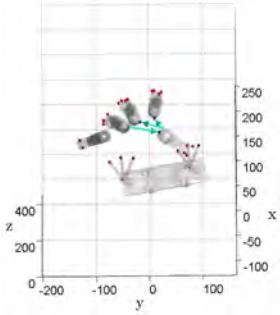

(i) Coin reconstruction.

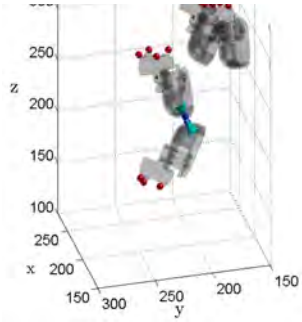

(j) Egg reconstruction.

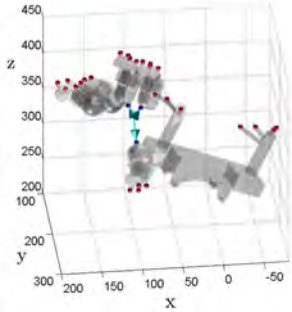

Fig. 5.20: Experimental Validation II: task execution (panels a-e) and reconstruction (panels f-j).

net torque on the bottle cap.

The fourth task consists in lifting a one dollar coin (mass 8 grams) placed on a small support. This task is challenging owing to the small size of the object to be grasped and to the precision of the operation involved. The possibility of lifting a coin while wearing the device is an indication of how the device does not hinder performing nimble operations.

Finally, the fifth task involves lifting an egg (mass 58.3 grams). As previously discussed, a limitation of our device is that while wearing a subject is prevent any direct cutaneous feedback. It is thus interesting to propose tasks that are challenging for what concerns force control. This is exactly the scope of this last task: lifting an egg without breaking it requires proper control of the forces applied by fingertips, and the fact that this task can be performed while wearing the device shows that it allows to retain a certain degree of precision.

The tasks described in this section were aimed to give a sample of the device versatility, and to show that despite the alteration of cutaneous feedback it is still possible to perform nimble tasks; deeper force analysis is demanded to future works.

Subject	Thimbles on	Bare fingers
1 (R)	p value: 1.17e-06 Multiple R-squared: 0.576 Adjusted R-squared: 0.561 $\alpha = -0.107$ $\beta = 9.86$	p value: 0.0113 Multiple R-squared: 0.208 Adjusted R-squared: 0.180 $\alpha = -0.0553$ $\beta = 8.68$
2 (R)	p value: 0.0293 Multiple R-squared: 0.159 Adjusted R-squared: 0.129 $\alpha = -0.0598$ $\beta = 12.4$	**p value: 0.0761** **Multiple R-squared: 0.108** **Adjusted R-squared: 0.0762** $\alpha = -0.0290$ $\beta = 6.26$
3 (R)	p value: 4.85e-08 Multiple R-squared: 0.661 Adjusted R-squared: 0.649 $\alpha = -0.131$ $\beta = 9.23$	**p value: 0.191** **Multiple R-squared: 0.0602** **Adjusted R-squared: 0.0266** $\alpha = -0.0160$ $\beta = 6.52$
4 (R)	p value: 7.33e-08 Multiple R-squared: 0.651 Adjusted R-squared: 0.638 $\alpha = -0.131$ $\beta = 8.50$	p value: 0.0218 Multiple R-squared: 0.174 Adjusted R-squared: 0.145 $\alpha = -0.0299$ $\beta = 6.70$
5 (R)	p value: 2.02e-05 Multiple R-squared: 0.483 Adjusted R-squared: 0.465 $\alpha = -0.103$ $\beta = 12.8$	p value: 4.84e-05 Multiple R-squared: 0.451 Adjusted R-squared: 0.431 $\alpha = -0.0943$ $\beta = 8.73$
6 (L)	p value: 5.70e-06 Multiple R-squared: 0.526 Adjusted R-squared: 0.510 $\alpha = -0.160$ $\beta = 12.8$	**p value: 0.128** **Multiple R-squared: 0.0837** **Adjusted R-squared: 0.0498** $\alpha = -0.0145$ $\beta = 5.24$
7 (L)	p value: 3.04e-05 Multiple R-squared: 0.468 Adjusted R-squared: 0.449 $\alpha = -0.141$ $\beta = 12.3$	p value: 0.0112 Multiple R-squared: 0.209 Adjusted R-squared: 0.181 $\alpha = -0.0606$ $\beta = 9.67$
8 (L)	p value: 4.53e-08 Multiple R-squared: 0.662 Adjusted R-squared: 0.650 $\alpha = -0.286$ $\beta = 17.8$	p value: 0.000102 Multiple R-squared: 0.422 Adjusted R-squared: 0.402 $\alpha = -0.0757$ $\beta = 9.84$

Table 5.5: Goodness of fit ($F = \alpha\ n_t + \beta$).
$p > 0.05$ in bold. (R) indicates right-handed subjects, while (L) indicates left-handed subjects.

Subject	Mean grip force (N)		p-value
	Thimbles on	Bare fingers	
1 (R) †	7.26±0.69	7.19±0.83	0.92
3 (R) *	5.94±0.43	6.33±0.60	0.0506
4 (R) *	5.33±0.70	6.06±0.57	0.0546
7 (L) *	8.9±0.71	8.56±0.81	0.471

Table 5.6: Steady state mean grip. Paired t-test was used for data marked with $*$, while Wilcoxon signed rank test was used for data marked with †. Normality was verified with Lilliefors test.

Subject	Thimbles on (second block)
4 (R)	p value: 1.64e-12
	Multiple R-squared: 0.580
	Adjusted R-squared: 0.572
	$\alpha = -0.074$
	$\beta = 10.87$

Table 5.7: Linear fit goodness for the 60-trials block.

Chapter 6

Conclusions

In this work we performed a complete validation of the wearable device ThimbleSense, which provides force measurements on fingertips together with an estimation of the position of contact points and was introduced in a previous work.

The validation was twofold. The first series of experiments focused on quantitatively evaluating measurement accuracy: for this purpose the device was tested under static and dynamic known loads, which in the worst conditions yielded errors of the order of 0.1 N for force measurements and 2 mm for contact point estimation.

In the last experiment we tackled a different problem, evaluating the distortion of cutaneous feedback, caused by wearing ThimbleSense over the fingertip, and its effects on grip force control. In particular, for a task which involved lifting an object with thumb and index of the right hand, we compared grip forces over a high number of trials in two different conditions: wearing the device on each fingers and having bare fingers. For all the participants in the experiment, both left and right handed, some learning was observed when wearing ThimbleSense, with a linear fit that was statistically significant for all subjects (including left-handed subjects). The analysis of the average grip force on the last trials gave mixed results: half of the subjects were able to reach (statistically) comparable forces for the two conditions, while the other half retained a higher force when wearing the thimbles. However, a final test with the subject that had retained the highest force, performed after several days, revealed an improved capability to control the grip force, which gives indication that it is possible to overcome these differences with training.

Now that a complete validation of the device has been performed, we plan to use ThimbleSense to study human grasp, after designing a training protocol to ensure containment of alteration of forces. However, other applications are

possible: in fact, with some minor modifications on the design, it is possible to apply this device as a way to measure forces on-the-fly for an existing robotic hand, without having to change the design of the hand itself.

Bibliography

[1] A. Bicchi, J. K. Slisbury, and D. L. Brock, "Contact sensing from force measurement," *The International Journal of Robotics Research*, vol. 12, pp. 249–262, 1993.

[2] M. Santello, M. Flanders, and J. F. Soechting, "Postural hand synergies for tool use," *The Journal of Neuroscience*, vol. 18, no. 23, pp. 10 105 – 10 115, 1998.

[3] M. Santello and J. F. Soechting, "Force synergies for multifingered grasping," *Experimental Brain Research*, vol. 133, no. 4, pp. 457 – 467, 2000.

[4] M. H. Schieber and M. Santello, "Hand function: peripheral and central constraints on performance," *Journal of Applied Physiology*, vol. 96, no. 6, pp. 2293 – 2300, 2004.

[5] M. G. Catalano, G. Grioli, E. Farnioli, A. Serio, C. Piazza, and A. Bicchi, "Adaptive synergies for the design and control of the pisa-IIT softhand," *International Journal of Robotics Research*.

[6] M. Bianchi, P. Salaris, A. Turco, N. Carbonaro, and A. Bicchi, "On the use of postural synergies to improve human hand pose reconstruction," in *Proceedings of IEEE Haptics Symposium*, 2012.

[7] M. Bianchi, P. Salaris, and A. Bicchi, "Synergy based optimal design of hand pose sensing," in *Proceedings of IEEE/RSJ International Conference on Intelligent Robots and Systems*, 2012.

[8] V. M. Zatsiorsky and M. L. Latash, "Multifinger prehension: An overview," *Journal of Motor Behavior*, vol. 40, no. 5, pp. 446–476, 2008.

[9] W. Zhang, A. M. Gordon, Q. Fu, and M. Santello, "Manipulation after object rotation reveals independent sensorimotor memory representations of digit positions and forces," *The Journal of Neurophysiology*, vol. 103, no. 6, pp. 2953 – 2964, 2010.

[10] L. Dipietro, A. M. Sabatini, and P. Dario, "A survey of glove-based systems and their applications," in *Proceedings of the 2008 IEEE Transactions on systems, man and cybernetics*, 2008.

[11] N. Sakai and S. Shimawaki, "Strain in the nail at fingertip compression," *Skin Research and Technology*, vol. 13, no. 4, pp. 449 – 453, 2007.

[12] M. Nakatani, K. Shiojima, S. Kinoshita, T. Kawasoe, K. Koketsu, and J. Wada, "Wearable contact force sensor system based on fingerpad deformation," in *Proceedings of the 2011 IEEE World Haptics Conference*, 2011.

[13] S. Mascaro and H. H. Asada, "Finger posture and shear force measurement using fingernail sensors: Initial experimentation," in *Proceedings of the 2001 IEEE International Conference on Robotics and Automation*, 2001.

[14] T. R. Grieve, J. M. Hollerbach, and S. A. Mascaro, "Force prediction by fingernail imaging using active appearance models," in *Proceedings of the 2013 IEEE World Haptics Conference*, 2013.

[15] G. Stillfried, U. Hillenbrand, M. Settles, and P. van der Smagt, "Mri-based skeletal hand movement model," in *The human hand - a source of inspiration for robotic hands*, R. Balaraman and V. Santos, Eds. Springer Tracts on Advanced Robotics, 2013.

[16] M. Gabiccini, G. Stillfried, H. Marino, and M. Bianchi, "A data-driven kinematic model of the human hand with soft-tissue artifact compensation mechanism for grasp synergy analysis," in *IEEE/RSJ International Conference on Intelligent Robots and Systems*, IROS 2013.

[17] MIT. Kinect hand detection. [Online]. Available: http://video.mit.edu/watch/kinect-hand-detection-12073/

[18] Tekscan. Grip system. [Online]. Available: http://www.tekscan.com/grip-pressure-measurement

[19] S. Mascaro and H. H. Asada, "Measurement of finger posture and three-axis fingertip touch force using fingernail sensors," *IEEE transactions on robotics and automation*, vol. 20, no. 1, pp. 26–35, 2004.

[20] T. R. Grieve, L. Lincoln, Y. Sun, J. M. Hollerbach, and S. A. Mascaro, "3d force prediction using fingernail imaging with automated calibration," in *Proceedings of IEEE Haptics Symposium*, 2010.

[21] T. R. Grieve, J. M. Hollerbach, and S. A. Mascaro, "Force prediction by fingernail imaging using active appearance models," in *Proceedings of IEEE World Haptics Conference*, 2013.

[22] S. J. Lederman and R. L. Klatzky, "Haptic identification of common objects: Effects of constraining the manual exploration process," *Perception & Psychophysics*, vol. 66, no. 4, pp. 618 – 628, 2004.

[23] ATI. F/t sensor: Nano17. [Online]. Available: http://www.ati-ia.com/products/ft/ft_models.aspx?id=Nano17

[24] D. W. Eggert, A. Lorusso, and R. B. Fisher, "Estimating 3-d rigid body transformations: a comparison of four major algorithms," *Machine Vision and Applications*, vol. 9, pp. 272 – 290, 1997.

[25] P. Space. Motion capture system. [Online]. Available: http://www.phasespace.com/

[26] Q. Fu, W. Zhang, and M. Santello, "Anticipatory planning and control of grasp positions and forces for dexterous two-digit manipulation," *The Journal of Neuroscience*, vol. 30, no. 27, pp. 9117 – 9126, 2010.

[27] E. Battaglia, G. Grioli, M. G. Catalano, M. Santello, and A. Bicchi, "Thimblesense: an individual-digit wearable tactile sensor for experimental grasp studies," in *Proceedings of IEEE International Conference on Robotics and Automation*, 2014 (forthcoming).

[28] G. Baud-Bovy and J. F. Soechting, "Two virtual fingers in the control of the tripod grasp," *Journal of Neurophysiology*, vol. 86, no. 2, pp. 604–615, 2001.